Double-humped phonon resonance in doubly resonant vibration systems: Phonon metamaterials analogy with doubly resonant electromagnetic structures

Lyudmila G. Potyomina [*]

Educational-scientific Institute of Physical Engineering, National Technical University "Kharkiv Polytechnic Institute",
2 Kirpichova str., 61002 Kharkiv, Ukraine

Phononic metamaterial which consists of two (or several) nanolayers separated by a planar defect of atomic-scale thickness is studied, under the assumption that the two-channel phonon interference mechanism of the transverse (cross-plane) heat flux control is dominant at high temperatures. An analytically exactly solvable discrete three-dimensional (3D) model of the multilayer interface between two semi-infinite bcc-lattice crystals is used to simulate phononic metamirror, metafilter, and meta-absorber. Two options of the general model in which two-path phonon interference reveals itself as double-humped resonance in the interface phonon absorption at weak dissipation or as total phonon transmission and total phonon reflection in the lossless limit are considered. An analogy is discussed between doubly resonant dissipative vibration systems and earlier investigated doubly resonant electromagnetic structure exhibiting both types of behavior: induced transparency and superscattering. It is shown that triple-peaked absorption resonance may arise from superposition of two-path phonon interference and Fabry-Pérot-type interference in the system with triple defect layer. The existence conditions of double-peaked and triple-peaked resonances as well as total interface absorption are analyzed in terms of nondissipative phonon scattering properties and dissipative parameters. Also additional peculiarities relevant to the thermal interface resistance problem are described. The study provides insight into heat management in phononic nanostructures and metamaterials like metamirrors, metafilters, and meta-absorbers.

I. INTRODUCTION

At present a large number of electromagnetic systems with different paths for an incoming wave to propagate have been studied completely [1–9]. Among these systems the most needed for practical applications are functional artificial metamaterials [2–7] such as photonic periodic nanostructures composed of metallic complexes embedded in optically transparent medium where localized plasmon resonances [8–11] can be excited, e.g., stereometamaterials arranged by stacked split-ring coupling resonators [12,13] or three-dimensional plasmon rulers [14]. In the planar versions of metamaterials, called metasurfaces or metafilms, the polarizable inclusions are arranged in two-dimensional (2D) arrays to achieve the desirable scattering properties. Metafilms may be filled with asymmetrical split-ring arrays [15], plasmonic oligomers [16–19], or with plane resonators of other shapes. Metasurfaces and bulk metamaterials may be fabricated on flexible substrates [20]. Utilizing a metal ground plane behind a thin absorbing metafilm [1,21–24] results in a perfect reflecting metasurface (metamirror) with a wide absorption band, whereas a periodic arrangement of different scale resonators in the foreground of dielectric substrate gives perfect multiband absorption [24]. An alternative way to build a full-power reflector (perfect metamirror) is to pack a metasheet without a back metal plane with appropriate electrically and magnetically polarizable (chiral bianisotropic, Huygens') inclusions [25], as well as a choice of specifically designed right- and left-handed helices as constituents in such a structure (Huygens' surface) permits us to create extremely thin perfect absorbers [26] (see also reviews [20,27] for details and relevant references). Similar wave scattering properties reveal themselves in completely nonmetallic metamaterials [27,28].

In all above systems and for each wave path an internal (initial) resonance frequency exists. The partial waves interfere constructively [resonant enhancement of the forward scattering (transmission), i.e., resonance] or destructively (resonant suppression of the transmission, i.e., resonant reflection, i.e., antiresonance). Among the simplest doubly resonant systems with two paths for an electromagnetic wave to propagate are structures, periodically modulated along one spatial dimension, e.g., ultrathin metal films [29] or dual dielectric structures with both short and long range periodicities [30].

Theoretical studies of multichannel interference phenomena use different methods, such as purely dynamical approach with or without consideration of dissipative effects, as well as the idea of cross section [9,31]. The concept of electromagnetic cross section suggests as the first step the introduction of leakage rates to avoid divergence. A transmission cross section is defined as the total transmitted power over the intensity of the incident plane wave. Further investigation is directed at finding the interference phase conditions for suppression or enhancement of the scattering cross section. Following this procedure a coupled-mode theory for a doubly resonant two-slits system [32] was recently developed to show

*potyomina@kpi.kharkov.ua

that electromagnetically induced transparency (EIT) and superscattering (antiresonance) can be observed depending on the excitation in a single structure. A model system used in Ref. [32] consists of two slits in a metal film illuminated by light on one side. Each slit can support a localized resonance, and hence the transmission cross section of the individual slit has a well-known Lorentzian line shape. The assumption that similar slits have approximately the same leakage rates and the spatial separation of the slits is small compared to the wavelength results in the conclusion that the eigenmodes have different damping factors, corresponding to superradiant and subradiant eigenmodes, whose contributions to the total cross section are regulated by the angle of incidence of the plane wave. From the above it follows that the interference phenomena in such an electromagnetic double-slit resonant structure (DSRS) are described with the help of five parameters and the angle of incidence.

At the same time, the resonance transmission and the resonance reflection due to multipath phonon interference are found experimentally [33] and described theoretically [34–40]. Thereby, one can raise a question about the phonon analog of DSRS. It may be, for example, a defect layer a few atoms in thickness embedded between two perfect crystals.

Earlier such a system has been studied within the frame of harmonic lattice dynamics [38–40], which is the simplest variant of atomistic approaches. In this theory the transmission coefficient of the phonons passing through an atomic-scale planar defect has the same definition as the electromagnetic transmission cross section. Even if dissipation is left out, the phonon scattering at the defect layer provides at its boundaries the phase shifts of the complex amplitudes of atom displacements, accompanying the reflected and transmitted phonons, relative to the phase of the incident phonon. These phase shifts have dynamical origin and in the case of a defect layer with two different channels for phonon transmission and two intrinsic frequencies, they result in both interference effects: total transmission (constructive interference resonance) and total reflection (destructive interference resonance) of the incident wave. Notably, for the study of phonon scattering from an intercalated impurity monolayer (or a few defect monolayers) between two semi-infinite crystal lattices, models of lattice dynamics are quite adequate to describe all phonon modes up to and including short-wave and high-frequency vibrations significant for high temperature heat transport. Accurate calculations of the thermal transmission across a single boundary between two mismatch solids [41–44] and through periodic nanostructures [45–49], already made in the framework of these models, are in good agreement with different experimental data on the cross-plane thermal conductivity in two-segment systems [43,50] as well as in the superlattices [47,51–53].

Thus, it is clear that the problem under discussion is directly related to the interface thermal resistance, often referred to as the Kapitza thermal boundary resistance. This Kapitza resistance creates a temperature drop across the interface between two dissimilar materials when a heat flux is applied. It was first observed between a solid material and liquid helium in 1941 [54]. More recently, the interface thermal resistance was found at solid-solid interfaces; relevant earlier studies are presented in the work of Swartz and Pohl in 1989 [50].

By now, phonon transport across interfaces between dissimilar crystals has been investigated in a considerable number of experimental and theoretical papers referred in textbooks [55–57] and reviews [50,58–62].

At present, it is well known that the interface thermal resistance depends on such parameters as the interface microstructure (roughness, disorder, dislocations, bonding), the material utilized, the temperature regime, and other factors, including inelastic phonon scattering at the interface. For the last two decades, in order to explain or to predict the experimental results on temperature discontinuity at the boundary between two dissimilar media, in particular, an inelastic scattering influence, it has been common to use methods based on the atomistic approaches: equilibrium and nonequilibrium molecular dynamics simulations [63–68] as well as equilibrium and nonequilibrium Green's function techniques [69–72].

Both these advanced methods have the following limitations. Molecular dynamics (MD) allows any type of anharmonic interatomic interactions and accounts for both elastic and inelastic phonon scattering at the interface through consideration of multiple-phonon processes, i.e., there are no restrictions on the mechanism of heat exchange between dissimilar media in contact [64,67]. As a rule, more realistic and more accurate numerical models are suggested when the analytically solvable theoretical models describing physical effects in the phonon transport control are not sufficient to explain the experimental data. In turn, advances in computing lead to new predictions in the thermal interface resistance investigations [63–68]. But MD simulations do not consider quantum effects and, because of this, are restricted to high temperatures.

By contrast, the atomistic Green's function technique is quantum mechanical. However to account for only a simple quadratic nonlinearity in the equations of motion of the atoms at solid-solid interface we need very cumbrous analytical calculations and also in the length scale where anharmonicity is of the second order. Despite these difficulties, an essential result was obtained in the Refs. [70,71]: Nonlinearity suppresses thermal transport across the interface even at moderately high temperatures. The effect of anharmonicity on the thermal interface resistance is discussed as well within the frame of the simplest atomistic lattice-dynamics approach in Refs. [43,45,47,68].

To study the role of inelastic phonon scattering on the thermal interface resistance in real experiments [73–77], the results from atomistic approaches are compared with those in the modifications of the traditionally used semiclassical diffuse mismatch model [50]: a joint frequency diffuse mismatch model [73], an anharmonic inelastic model [74], a higher harmonic inelastic model [75], an inelastic phonon radiation limit [76] (see also Ref. [77]).

Current progress in the semiconductor nanotechnologies provides creation of new advanced engineered materials for using at continuous scaling down in high-power nanoelectronics. The new opportunities stimulate the search for other more efficient heat removal techniques to control the increasing power density in materials both with extremely high and extremely low thermal conductivity.

In this respect, a perfect crystal divided into halves (or into several nanolayers) by a planar defect of atomic-scale thickness is proposed to use for heat flux control in nanoscale at high temperatures, provided that two-channel (or two-path) phonon interference mechanism is dominant in the energy transfer. In such systems the role of interface inelastic scattering in the cross-plane phonon transmission has to be of the same importance as in the classical problem of the thermal interface resistance for the dissimilar media. Further in this paper, the phenomena of two-path phonon interference are studied on the base of a model, described in the previous work [40]. In this model the interface scattering of one incident phonon results in only one transmitted bulk phonon and only one reflected bulk phonon whose amplitudes are defined by the multipath interference of the partial waves passing through different channels within the defect area only. No localized defect vibration eigenmodes exist unlike the doubly resonant electromagnetic structure [32] in which either of the two slits can support a localized resonance.

Two types of vibration systems (doubly and thrice resonant) in the context of the discrete scalar model are considered. One of these systems has a checkerboard-type defect monolayer (doubly resonant CB model), in which the impurities of two sorts alternate in staggered order and interact only with their nearest neighbors in the harmonic approximation. The other model is a system with a triple defect layer (thrice resonant TL model), consisting of three homogeneous impurity monolayers: The intermediate layer is in between two identical outer defect layers, interacting directly through the next-to-nearest-neighbor elastic force, besides their basic elastic coupling with nearest neighboring atoms.

It is shown that the simplest counterpart of DSRS in the phonon dynamics is the CB model. In the nondissipative CB model the phonon transmission peculiarities (resonance and antiresonance) depend on two intrinsic frequencies and two defect force constants. It should seem that these four parameters correspond to two localized resonances and two leakage rates in DSRS [32]. But in the couple-mode theory of DSRS two additional values were entered into consideration: direct and indirect coupling between the resonances. It is apparent that in order to be the most convenient counterpart of DSRS the CB model must include the local energy dissipation within both phonon transmission channels as two additional parameters. It means that phonon analog of DSRS is inverse to electromagnetic couple-mode theory for DSRS in such a sense that the roles of parameters change over. In other words, to study a doubly resonant vibration systems (DRVS) as a phonon analog of the electromagnetic double-slit resonant structure (DSRS) from Ref. [32] it is necessary to change paradigm.

In the present work we analyze a spectral interface absorption behavior of DRVS analogous to a spectral behavior of a cross section in DSRS characterized by two resonances: a broad one and a narrow one. In such cases local maxima of the phonon absorption fall on the frequencies where the scattering coefficients of the corresponding nondissipative case show a steep decline, steeper curve corresponding to narrow absorption resonance. The position of this narrow resonance with respect to the broad peak remains approximately unchanged as the weak local dissipation is varied in DRVS by analogy

with DSRS where resonance frequency locations are not dependent of the angle of light incidence. An exact expression of the interface phonon absorption is presented here approximately as the sum of the contributions from the absorption in either phonon channel and from dissipative motion of the boundary planes.

The second model, the TL model, exhibits similar behavior and also reveals properties different from those in the CB model. Thus, a phenomenon of triple-peaked absorption resonance may occur in the vibration system with two-path phonon interference if triple defect layer is filled by fairly heavy atoms and has weak coupling with adjacent host layers. Such a system with three nondissipative total transmission frequencies and three intrinsic frequencies produces dual interference picture in which two-path phonon interference and phonon analog of the Fabry-Pérot-type interference superpose. In another case, when the intrinsic frequency of two tightly bound dense outer layers is close to that of a weakly bound inner layer, anomalous total interface absorption should be expected. The third distinctive feature of the TL model as compared to the CB model is that the narrow peak may exchange places with a broad peak in two close cases with defect atoms little different in the material constants. From the results obtained on the interfacial two-channel phonon transmission it follows that within certain frequency ranges the weak dissipation taken into account may lead to energy redistribution between scattered and transmitted energy fluxes and also phonon energy interface absorption in such a way that the heat transport has to be either suppressed or increased.

The paper is organized as follows. Section II contains a brief description of the general theoretical model for phonon scattering by triple defect layer covering all simple cases of two-path phonon interference under present consideration. In Sec. III the resonance phonon interface absorption by the checkerboard-type impurity monolayer intercalated between two crystals (CB model) is discussed as a spectral analog of doubly resonant electromagnetic system behavior and as a mechanism of first importance in the thermal interface resistance control.

Section IV presents an investigation of another vibration system which is thrice resonant on condition of two-path interference: the TL model with the two-dimensional triple defect layer homogeneous along its plane. In this model, more complex interference peculiarities are analyzed and the criterion for total absorption maximum is obtained. Finally, the main conclusions are given in Sec. V.

II. BRIEF DESCRIPTION OF CRYSTAL MODEL WITH TRIPLE DEFECT LAYER

Following Ref. [40], a bcc lattice with planar triple defect layer embedded between two semi-infinite crystals is considered. A fragment of this structure is shown in Fig. 1. Lines interconnecting nodes indicate cell borders. Circles at the centers and sites of the cells are different sorts of atoms. Lines between centers and sites as well as between two centers symbolize nearest-neighbor and next-to-nearest-neighbor bonds. The atom position is specified by three integers p_i, $i = 1, 2, 3$. Numbering along the defect plane and across it is carried out with $p_{1,2}$ and p_3, respectively. Even integers
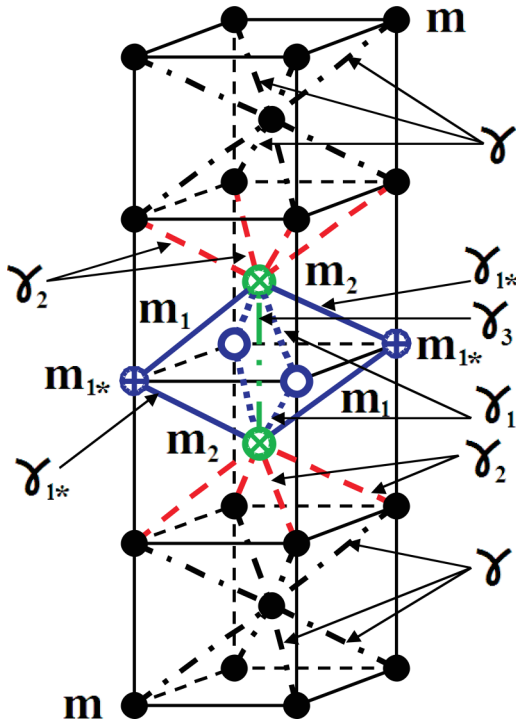
FIG. 1. General model.

The equations of lattice dynamics can be presented in the following form:

$$m\ddot{u}_{p_1}^{p_2,p_3} = -\gamma \sum_{\delta_i} \Phi_{\delta_1}^{\delta_2,\delta_{\delta_3}}, \quad |p_3| \geqslant 3, \tag{1}$$

where

$$\Phi_{\delta_1}^{\delta_2,\delta_3} = u_{p_1}^{p_2,p_3} - u_{p_1+\delta_1}^{p_2+\delta_2,p_3+\delta_3}, \tag{2}$$

$p_{1,2,3}$ are the triplets of even and odd integers; the index δ_i at the summation symbol means that the summation is over eight combinations of $\delta_1, \delta_2, \delta_3 = \pm 1$;

$$m\ddot{u}_{2n_1}^{2n_2,2\delta_3} = -\sum_{\delta_{1,2}} (\gamma \Phi_{\delta_1}^{\delta_2} + \gamma_2 \bar{\Phi}_{\delta_1}^{\delta_2}), \tag{3}$$

where

$$\Phi_{\delta_1}^{\delta_2} = u_{2n_1}^{2n_2,2\delta_3} - u_{2n_1+\delta_1}^{2n_2+\delta_2,3\delta_3},$$
$$\bar{\Phi}_{\delta_1}^{\delta_2} = u_{2n_1}^{2n_2,2\delta_3} - u_{2n_1+\delta_1}^{2n_2+\delta_2,\delta_3}, \tag{4}$$

the index $\delta_{1,2}$ at the summation symbol implies the summation over four possible combinations of $\delta_1, \delta_2 = \pm 1$;

$$m_1\ddot{u}_{2n_1+2}^{2n_2,0} = -\gamma_1 \sum_{\delta_i} (u_{2n_1+2}^{2n_2,0} - u_{2n_1+2+\delta_1}^{2n_2+\delta_2,\delta_3}), \tag{5}$$

$$m_{1*}\ddot{u}_{2n_1}^{2n_2,0} = -\gamma_{1*} \sum_{\delta_i} (u_{2n_1}^{2n_2,0} - u_{2n_1+\delta_1}^{2n_2+\delta_2,\delta_3}), \tag{6}$$

and

$$m_2\ddot{u}_{2n_1+1}^{2n_2+1,\delta_3} = -\gamma_2 \sum_{\delta_{1,2}} \tilde{\Phi}_{\delta_1}^{\delta_2} - \gamma_1\Phi_1 - \gamma_{1*}\Phi_{1*} - \delta_3\gamma_3\Phi_3, \tag{7}$$

where

$$\tilde{\Phi}_{\delta_1}^{\delta_2} = u_{2n_1+1}^{2n_2+1,\delta_3} - u_{2n_1+1+\delta_1}^{2n_2+1+\delta_2,2\delta_3},$$
$$\Phi_1 = 2u_{2n_1+1}^{2n_2+1,\delta_3} - u_{2n_1}^{2n_2+2,0} - u_{2n_1+2}^{2n_2,0},$$
$$\Phi_{1*} = 2u_{2n_1+1}^{2n_2+1,\delta_3} - u_{2n_1+2}^{2n_2+2,0} - u_{2n_1}^{2n_2,0},$$
$$\Phi_3 = u_{2n_1+1}^{2n_2+1,1} - u_{2n_1+1}^{2n_2+1,-1}. \tag{8}$$

These equations describe, respectively, the vibrations of the host atoms in planes $|p_3| \geqslant 3$ and $p_3 = \pm 2$ [Eqs. (1) and (3)], the vibrations of impurities in plane $p_3 = 0$ [Eqs. (5) and (6)], and the vibrations of impurities in planes $p_3 = \pm 1$ [Eq. (7)].

To understand the key features of the resonance interface absorption discussed in the present work the phonon propagation in the direction perpendicular to the defect layer is considered. In this case, under the assumption that the half length of the bcc cell edge is 1, one obtains from Eq. (1) the bulk phonon spectrum in the host material, i.e., the dependence of the phonon frequency ω on the one-dimensional normalized wave vector $k > 0$:

$$\omega = \omega_{\text{ph}} \sin(k/2), \tag{9}$$

where $\omega_{\text{ph}} = 4\sqrt{\gamma/m}$. The host lattice parameters γ and m define the upper limit of the resonance frequency which must be smaller than the maximum phonon frequency ω_{ph}. By Eq. (9) the maximum frequency is on the Brillouin zone edge.

The reflection R and transmission T coefficients of phonons incident onto defect planes $p_3 = 0, \pm 1$ are defined as $R = |a_R|^2$ and $T = |a_T|^2$, where a_R and a_T are the amplitudes

$p_i = 2n_i$, where $i = 1, 2, 3$, correspond to cell sites and odd integers $p_i = 2n_i + 1$, where $i = 1, 2, 3$, to cell centers. Host atoms with masses m (black circles) are indexed by triplets $(2n_1, 2n_2, 2n_3)$, where $n_3 \neq 0$, and $(2n_1 + 1, 2n_2 + 1, 2n_3 + 1)$, where $n_3 \neq 0, -1$. The defect region consists of three atomic planes $p_3 = 0, \pm 1$. Impurities with masses m_1 (empty circles) and m_{1*} (circular rings of the oplus type) lie in plane $p_3 = n_3 = 0$ at cell sites and are labeled, respectively, by $(2n_1 + 2, 2n_2, 0)$ and $(2n_1, 2n_2, 0)$. Impurities with masses m_2 (circular rings of the otimes type) take positions $(2n_1 + 1, 2n_2 + 1, \pm 1)$.

Below the atom displacements are assumed to be one-component and directed perpendicular to the defect planes. The displacement of an atom in position (p_1, p_2, p_3) is denoted by $u_{p_1}^{p_2,p_3}$. All three p_i in each triplet of indices are either even or odd, i.e., either $p_i = 2n_i$ or $p_i = 2n_i + 1$ for $i = 1, 2, 3$.

As a first approximation, the nearest-neighbor interaction is taken into account—namely, the interaction between an atom at the cell center and its nearest eight neighbors at lattice nodes. The force constant γ characterizes the interaction between host atoms. The symbols γ_1 and γ_{1*} stand for the force constants of nearest-neighbor interactions between impurities $m_1 \longleftrightarrow m_2$ and $m_{1*} \longleftrightarrow m_2$, respectively. The force constant γ_2 characterizes the nearest-neighbor interaction between host atoms and impurities m_2. Besides, the next-to-nearest-neighbor interaction with the force constant γ_3 between the impurities m_2 in the opposite layers is allowed for. Below, for the sake of convenience, all the above force constants are assumed to characterize the interaction along the direction perpendicular to the defect planes.

of the displacements $u_{p_1,R}^{p_2,p_3}$ and $u_{p_1,T}^{p_2,p_3}$ of the reflected and transmitted phonons, respectively. The amplitude of the displacement associated with the incident phonon $u_{p_1,I}^{p_2,p_3}$ equals to 1. It is assumed that the incident phonon propagates with wave vector $k > 0$ in the part of the lattice where the indices p_3 are negative, so the phase factors take the form $\exp[i(\pm kp_3 - \omega t)]$, where the upper sign corresponds to the incident and transmitted phonons and the lower sign appropriates to the reflected phonon.

The expressions for complex reflection a_R and transmission a_T amplitudes may be found after substitution of the displacements of host atoms

$$u_{p_1}^{p_2,p_3} = [\exp(ikp_3)$$
$$+ a_R \exp(-ikp_3)] \exp(-i\omega t), \quad p_3 < -1,$$
$$u_{p_1}^{p_2,p_3} = a_T \exp[i(kp_3 - \omega t)], \qquad p_3 > 1,$$

into Eqs. (1)–(8). According to Ref. [40], the simple calculations give $a_{R,T}$ in the form

$$a_R = -\frac{e^{-i4k}}{2}\left[\frac{\Lambda^{(-)}}{\Lambda_*^{(-)}} + \frac{\Lambda^{(+)}}{\Lambda_*^{(+)}}\right], \tag{10}$$

$$a_T = \frac{e^{-i4k}}{2}\left[\frac{\Lambda^{(-)}}{\Lambda_*^{(-)}} - \frac{\Lambda^{(+)}}{\Lambda_*^{(+)}}\right], \tag{11}$$

where

$$\Lambda^{(\pm)} = A + \frac{16\gamma_2^2}{B^{(\pm)}}, \quad \Lambda_*^{(\pm)} = A^* + \frac{16\gamma_2^2}{B^{(\pm)}},$$

$$A = 0.5m\omega^2 - 4\gamma_2 - i4\gamma \sin k,$$

$$B^{(-)} = 2(\gamma_1 + \gamma_{1*} + \gamma_3 + 2\gamma_2) - m_2\omega^2,$$

$$B^{(+)} = B^{(-)} - 2\gamma_3 + 2B,$$

$$B = \frac{\gamma_1\omega_1^2}{\omega^2 - \omega_1^2} + \frac{\gamma_{1*}\omega_{1*}^2}{\omega^2 - \omega_{1*}^2}, \tag{12}$$

and

$$\omega_1 = 2\sqrt{2\gamma_1/m_1}, \quad \omega_{1*} = 2\sqrt{2\gamma_{1*}/m_{1*}} \tag{13}$$

are the intrinsic frequencies attributed to the defects lying in plane $p_3 = 0$. The asterisk at A means complex conjugation. If all constants are real, then $\Lambda_*^{(\pm)} = \Lambda^{(\pm)*}$ and the equality $T + R = 1$ holds true.

In the general case the proposed vibration system falls into the category of fourfold resonant due to three intrinsic frequencies corresponding to three paths for phonon transmission across the defect—namely, two paths through different impurities in the plane $p_3 = 0$ and a third path through the next-to-nearest-neighbor interatomic bond γ_3 between impurities in the planes $p_3 = \pm 1$ (Fig. 1). The fourth intrinsic frequency is associated with one-channel phonon transmission between triple defect layer and each adjacent layer $p_3 = \pm 2$ through interatomic bond γ_2. Accordingly, four total transmission frequencies $\omega = \omega_T$ may be found as four roots of biquartic equation resulting from Eqs. (10) and (12) at $a_R = 0$. Generally the frequencies ω_T depend on parameters of the adjacent layers $p_3 = \pm 2$ [see, e.g. Eqs. (24) and (25)]. This points to the fact that resonance phonon propagation is due to the synchronism in the motion of the defect atoms with the motion of their neighboring host atoms. At the same

time, from Eqs. (11) and (12) it follows that $a_T = 0$ at two antiresonance frequencies $\omega = \omega_R$ which obey the biquadratic equation

$$\frac{\gamma_1\omega_1^2}{\omega_R^2 - \omega_1^2} + \frac{\gamma_{1*}\omega_{1*}^2}{\omega_R^2 - \omega_{1*}^2} - \gamma_3 = 0. \tag{14}$$

In accordance with Eq. (14), ω_R is independent of the mass m_2 of impurities in planes $p_3 = \pm 1$ and of the force constant γ_2 specifying the interaction of these impurities with host atoms. It means that Eq. (14) for the total reflection frequencies presents an equality of the energy fluxes, which pass across the defect layer in opposite directions only through the inner parallel channels.

From this point on we will consider the systems with two-path phonon interference and only one antiresonance frequency ω_R. The first system contains checkerboard-type monolayer of the simplest structure with four defect parameters—namely, force constants γ_1 and γ_{1*} and impurity masses m_1 and m_{1*} (or intrinsic frequencies ω_1 and ω_{1*}). This model is designated as the checkerboard-type (CB) model. In the CB model antiresonance frequency ω_R is defined by Eq. (14) at $\gamma_3 = 0$. In the second simple system a triple defect layer consists of three homogeneous monolayers. In this case one antiresonance frequency ω_R is the root of Eq. (14) with parameters $\gamma_1 = \gamma_{1*}$ and $\omega_1 = \omega_{1*}$, determining homogeneous inner layer. This model is referred to as the triple-defect-layer (TL) model.

In both models two different paths for phonon transmission exist only within the very thin defect layer. However, it is impossible to excite local vibrations of the planar defect if the bulk crystal is at rest, i.e., no localized eigenmodes exist in contrast to the motion of free oscillators [78], whose eigenfrequencies (e.g., ω_1 and ω_{1*}) are used as intrinsic frequencies. An interface scattering of an incident phonon leads to formation of one transmitted and one reflected waves whose amplitudes are defined by two-path phonon interference and Fabry-Pérot-type interference. It is correct to treat these waves as a collective mode appearing in the crystal with a planar defect under incidence of a plane wave. In a particular case the collective mode can switch from a total transmission mode to a total reflection mode depending on the incoming wave frequency. Such significant changes of the collective mode are due to specific dynamics of the defect atoms, which is very sensitive to local weak dissipation. That is why the effect of local weak dissipation on collective dynamic motion and interface energy absorption may be of essential interest for investigations of the thermal interface resistance and will be studied below on the basis of the conventional phenomenological approach [78]. In this approach local weak dissipation is taken into account by adding a small imaginary component γ_i' in the defect force constants γ_i. Namely, for the general model (Fig. 1) the real force constants γ_i ($i = 1, 1*, 2, 3$) in Eqs. (10)–(13) have to be replaced by the complex values $\gamma_i \rightarrow \gamma_i - i\gamma_i'$. In particular cases, this problem is considered in Sec. III B and Sec. IV more fully.

In what follows, an analogy is discussed between doubly resonant dissipative vibration systems and the earlier investigated doubly resonant electromagnetic structure [32]. The connection between double-humped resonance in the
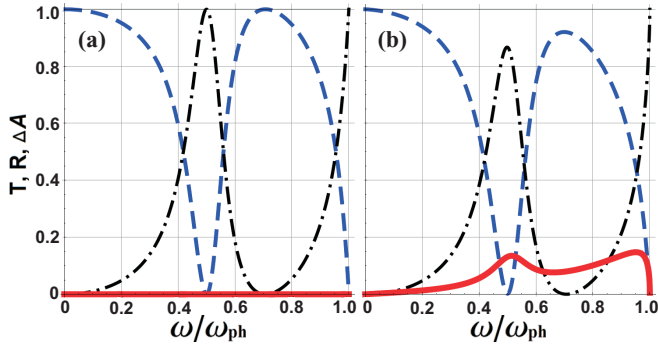
FIG. 2. Spectra of phonon energy transmission T (dashed line), reflection R (dotted-dashed line), and absorption ΔA (solid line) versus reduced frequency $\omega/\omega_{\text{ph}}$ at a checkerboard-type defect layer with parameters $m_2 = m$, $\gamma_2 = \gamma_1 = \gamma_{1*} = \gamma$, $m_{1*} = m$ and impurity mass $m_1 = 3m$ for the cases: (a) without dissipation, (b) with dissipative parameters $\gamma'_1 = \gamma'_{1*} = 0.014\gamma$, intrinsic frequencies $\omega_1 = \omega_{\text{ph}}/\sqrt{6}$ and $\omega_{1*} = \omega_{\text{ph}}/\sqrt{2}$.

interface phonon absorption at weak dissipation on one hand, and total phonon transmission and total phonon reflection in the lossless limit under two-path phonon interference on the other hand, is analyzed. It is shown that resonance transmission frequencies, resonance reflection frequencies, and resonance absorption frequencies do not always coincide with the intrinsic frequencies. It is demonstrated that triple-peaked absorption resonance arises from superposition of two-path phonon interference and Fabry-Pérot-type interference in the system with triple defect layer. Also, total interface absorption and other peculiarities relevant to the thermal interface resistance problem are described.

Namely, it will be seen that availability of two-path phonon interference antiresonance in the lossless phonon spectrum does not assure noticeable interface absorption at weak dissipation taken into account, such as in the case of checkerboard-type defect layer filled with host atoms and heavy impurities (Fig. 2). On the other hand, the single interface absorption resonance may be due to different reasons. For example, in the case of single homogeneous light impurity monolayer weakly bound with host atoms at both opposite boundaries (provided that these boundaries interact through an extremely weak direct next-to-nearest-neighbor bonds) a phonon transmission may be considered as one-path. This situation is characterized by nondissipative narrow transmission resonance [Fig. 13(c)] and pronounce single absorption resonance [Fig. 13(d)] when the weak dissipation is allowed for. Similar absorption spectra are realized also in the systems with two-path phonon interference [Figs. 3(b), 6(d), 13(b), and 14(b); see also Figs. (b+), 6(d+), 13(b), and 14(b) in Ref. [79]].

III. RESONANCE PHONON SCATTERING BY CHECKERBOARD-TYPE IMPURITY MONOLAYER INTERCALATED BETWEEN TWO CRYSTALS (CB MODEL)

A. Two-channel phonon interference in nondissipative checkerboard-type model

As already noted, in the CB model a defect plane, embedded in a crystal, consists of two types of impurities alternating
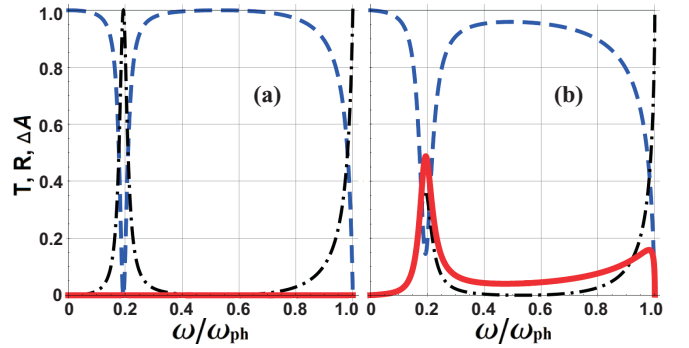

FIG. 3. Spectra of phonon energy transmission T (dashed line), reflection R (dotted-dashed line), and absorption ΔA (solid line) versus reduced frequency $\omega/\omega_{\text{ph}}$ at a checkerboard-type defect layer with parameters $m_2 = m$, $\gamma_2 = \gamma$, $\gamma_1 = 0.14\gamma$, $\gamma_{1*} = 1.8\gamma$, and impurity masses $m_1 = m_{1*} = 2m$ for the cases: (a) without dissipation, (b) with dissipative parameters $\gamma'_1 = 0.014\gamma$, $\gamma'_{1*} = 0.018\gamma$; intrinsic frequencies $\omega_1 \approx 0.187\omega_{\text{ph}}$ and $\omega_{1*} \approx 0.671\omega_{\text{ph}}$.

in staggered order. It is assumed that all defect masses m_1, m_{1*} and elastic constants γ_1, γ_{1*}, coupling the impurities with the boundary host atoms with $m_2 = m$, $\gamma_2 = \gamma$, are different and there is no interaction between boundary planes $p_3 = \pm 1$ [see Eqs. (1)–(8) and Fig. 1 at $\gamma_3 = 0$, $m_2 = m$, $\gamma_2 = \gamma$]. The force constants γ_1 and γ_{1*} are taken to be real unless dissipation in the defect layer is non-negligible.

In this model two channels of the phonon propagation through the defect plane exist already in the nearest-neighbor approximation. One of them passes through the impurity bond γ_1 and the other runs across the impurity bond γ_{1*}. In such a situation, the expressions (10) and (11) for the reflection and transmission amplitudes can be written as follows:

$$a_R = \frac{N_r(\omega)\exp(-2ik)}{D_{\text{CB}}(\omega)[4\gamma\exp(ik) - B_{\text{CB}}^{(-)}]}, \qquad (15)$$

$$a_T = \frac{N_t(\omega)\exp(-2ik)}{D_{\text{CB}}(\omega)[4\gamma\exp(ik) - B_{\text{CB}}^{(-)}]}, \qquad (16)$$

where

$$
\begin{aligned}
N_r(\omega) = &-2\omega\{2(2\gamma - \gamma_1 - \gamma_{1*})\omega^4 - \omega^2[2(2\gamma \\
&- \gamma_1 - \gamma_{1*})(\omega_1^2 + \omega_{1*}^2) + \gamma_1\omega_1^2 + \gamma_{1*}\omega_{1*}^2 \\
&- \omega_{\text{ph}}^2(\gamma_1 + \gamma_{1*})^2/4\gamma] + \omega_1^2\omega_{1*}^2(4\gamma - \gamma_1 - \gamma_{1*}) \\
&- \omega_{\text{ph}}^2(\gamma_1 + \gamma_{1*})(\gamma_1\omega_{1*}^2 + \gamma_{1*}\omega_1^2)/4\gamma\},
\end{aligned}
\qquad (17)
$$

$$
\begin{aligned}
N_t(\omega) = 2i\sqrt{\omega_{\text{ph}}^2 - \omega^2}[\omega^2(\gamma_1\omega_1^2 + \gamma_{1*}\omega_{1*}^2) \\
- \omega_1^2\omega_{1*}^2(\gamma_1 + \gamma_{1*})],
\end{aligned}
\qquad (18)
$$

$$
\begin{aligned}
B_{\text{CB}}^{(-)} = 4\gamma\exp(ik) - \frac{8\gamma\omega}{\omega_{\text{ph}}^2}\left(i\sqrt{\omega_{\text{ph}}^2 - \omega^2} + \omega\right) \\
+ 2(\gamma_1 + \gamma_{1*}),
\end{aligned}
\qquad (19)
$$

$$
\begin{aligned}
D_{\text{CB}}(\omega) = &i\sqrt{\omega_{\text{ph}}^2 - \omega^2}(\omega^2 - \omega_1^2)(\omega^2 - \omega_{1*}^2) + \omega\{\omega^4 \\
&- \omega^2[\omega_1^2 + \omega_{1*}^2 + \omega_{\text{ph}}^2(\gamma_1 + \gamma_{1*})/4\gamma] \\
&+ \omega_1^2\omega_{1*}^2 + \omega_{\text{ph}}^2(\gamma_1\omega_{1*}^2 + \gamma_{1*}\omega_1^2)/4\gamma\}.
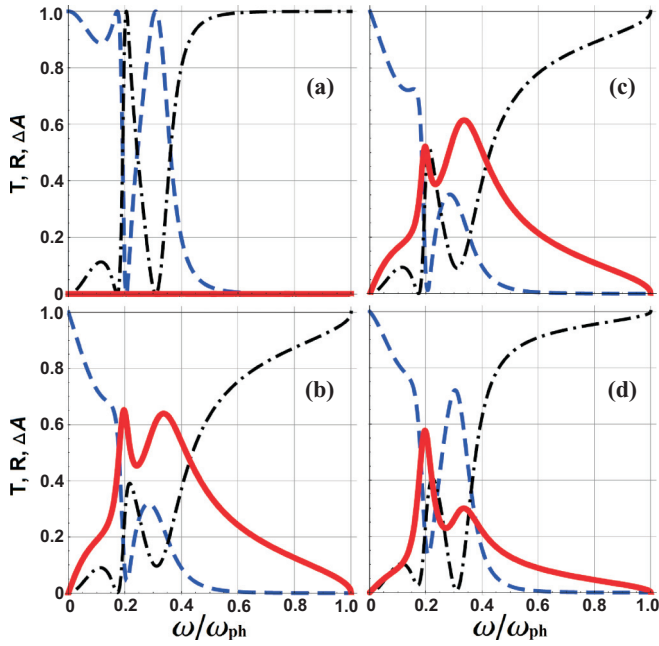\end{aligned}
\qquad (20)
$$

FIG. 4. Spectra of phonon energy transmission T (dashed line), reflection R (dotted-dashed line), and absorption ΔA (solid line) versus reduced frequency ω/ω_{ph} at a checkerboard-type defect layer with parameters $m_2 = m$ and $\gamma_2 = \gamma$, impurity masses $m_1 = m_{1*} = 2m$, elastic force constants $\gamma_1 = 0.14\gamma$ and $\gamma_{1*} = 0.4\gamma$ (intrinsic frequencies $\omega_1 \approx 0.187\omega_{ph}$ and $\omega_{1*} \approx 0.316\omega_{ph}$) for the cases: (a) without dissipation, (b), (c), and (d) are the cases with phonon energy absorption, dissipative parameters in (b) $\gamma_1' = 0.012\gamma$, $\gamma_{1*}' = 0.1\gamma$, in (c) $\gamma_1' = 0.006\gamma$, $\gamma_{1*}' = 0.09\gamma$, and in (d) $\gamma_1' = \gamma_{1*}' = 0.02\gamma$.

Here, the symbol ω_{ph} denotes the maximum phonon frequency for normal incidence in view of Eq. (9) and the intrinsic frequencies ω_1 and ω_{1*} are defined by Eqs. (13). Below the symbol ω_1 refers to the minor intrinsic frequency.

According to Eq. (14), the total reflection frequency ω_R (transmission antiresonance) is determined by the expression:

$$\omega_R = \omega_1 \omega_{1*} \sqrt{\frac{\gamma_1 + \gamma_{1*}}{\gamma_1 \omega_1^2 + \gamma_{1*} \omega_{1*}^2}}. \qquad (21)$$

If $\Delta\omega = \omega_{1*} - \omega_1 \ll \omega_1$, from Eq. (21) we get an estimate for the resonance frequency

$$\omega_R \approx \frac{\omega_1 + \omega_{1*}}{2} + \frac{\Delta\omega(\gamma_1 - \gamma_{1*})}{2(\gamma_1 + \gamma_{1*})}. \qquad (22)$$

From Eq. (21) it follows that once one type of impurities with mass m_1 is weakly bound, i.e., $\gamma_1 \ll \gamma_{1*}$ and $\gamma_1 \omega_1^2 \ll \gamma_{1*}\omega_{1*}^2$, then $\omega_R \gtrsim \omega_1$ and zero-transmission dip is observed close to the minor intrinsic frequency ω_1. As it also follows from Eq. (21), in the nondissipative case at arbitrary defect parameters the restriction $\omega_1 < \omega_{1*} < \omega_{ph}$ is sufficient to fulfill the inequality $\omega_1 < \omega_R < \omega_{1*} < \omega_{ph}$. To study double-resonance dissipative interference this case seems to be the most interesting and will be examined hereafter. Dependencies of the scattering coefficients $R = |a_R|^2$ and $T = |a_T|^2$ versus reduced frequency ω/ω_{ph} are shown in Figs. 2–7.

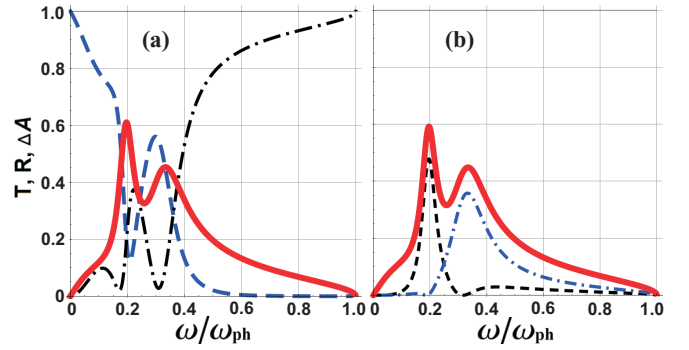From formulas (15) and (17) it is evident that two transmission maxima in Figs. 4(a), 6(a), 6(c), and 7(a) correspond

FIG. 5. Phonon energy absorption ΔA (solid line) versus reduced frequency ω/ω_{ph} at a checkerboard-type defect layer with the same parameters as in Fig. 4(a) and dissipative parameters $\gamma_1' = 0.02\gamma$ and $\gamma_{1*}' = 0.04\gamma$: (a) an exact calculation by the formula (29), coefficients of phonon energy transmission T (dashed line), and reflection R (dotted-dashed line); (b) approximate calculations $\Delta A \approx \Delta A_2 + \Delta A_1 + \Delta A_{1*}$ by the formulas (30)–(32), ΔA_1 (dashed line) is absorption due to viscous motion of the defect mass m_1, and ΔA_{1*} (dotted-dashed line) is absorption in the parallel channel with the defect mass m_{1*}; ΔA_2 is depicted in Fig. 5 in Ref. [79].

to two roots (ω_{T1} and ω_{T2}) of the equation:

$$2(2\gamma - \gamma_1 - \gamma_{1*})\omega_T^4 - \omega_T^2\big[2(2\gamma - \gamma_1 - \gamma_{1*})(\omega_1^2 + \omega_{1*}^2)$$
$$+ \gamma_1\omega_1^2 + \gamma_{1*}\omega_{1*}^2 - \omega_{ph}^2(\gamma_1 + \gamma_{1*})^2/4\gamma\big]$$
$$+ \omega_1^2\omega_{1*}^2(4\gamma - \gamma_1 - \gamma_{1*})$$
$$- \omega_{ph}^2(\gamma_1 + \gamma_{1*})(\gamma_1\omega_{1*}^2 + \gamma_{1*}\omega_1^2)/4\gamma = 0. \qquad (23)$$

One of the simplest CB models is a perfect crystal of argon (Ar) with a defect plane filled with host atoms and their heavy isotopes in checker order. This system is investigated in Ref. [38] to describe the so-called "isotopic defect" in the nondissipative limit without considering bond defects, i.e., with only one defect parameter m_1. In such a case, depicted in Fig. 2(a) at $m_2 = m$ and $\gamma_2 = \gamma$, both the total transmission frequency ω_T and total reflection frequency ω_R manifest themselves, both intrinsic frequencies are less than ω_{ph} and the relation $\omega_1 < \omega_R < \omega_{1*} < \omega_{ph}$ is realized. The major intrinsic frequency ω_{1*} is equal to the single total transmission frequency $\omega_T = \omega_{1*} = \omega_{ph}/\sqrt{2}$ and corresponds to the double minimum bulk phonon length.

In the CB model with the defect plane occupied by the weakly bound ($\gamma_1 \ll \gamma$) and not-too-heavy ($m_1 \sim m$) impurities alternating with the host atoms ($m_{1*} = m$, $\gamma_{1*} = \gamma$) one can obtain from Eq. (23) approximate analytical expressions—for total transmission low frequency ω_{T1}

$$\omega_{T1} \simeq \omega_1(1 - m_1/5m)^{1/2} \qquad (24)$$

and for total transmission high frequency ω_{T2}

$$\omega_{T2} \simeq \omega_{ph}(5/8)^{1/2}(1 - \gamma_1/50\gamma), \qquad (25)$$

the major frequency ω_{T2} being almost independent of the parameters γ_1 and m_1. Such independence is similar to the case of heavy impurities with only one defect parameter [Fig. 2(a)], but now the frequency ω_{T2} does not coincide with major intrinsic frequency $\omega_{1*} = \omega_{ph}/\sqrt{2}$ which is less than ω_{T2}, i.e., $\omega_{1*} < \omega_{T2}$ (we recall that the atoms at the planes $p_3 = \pm 1$ in
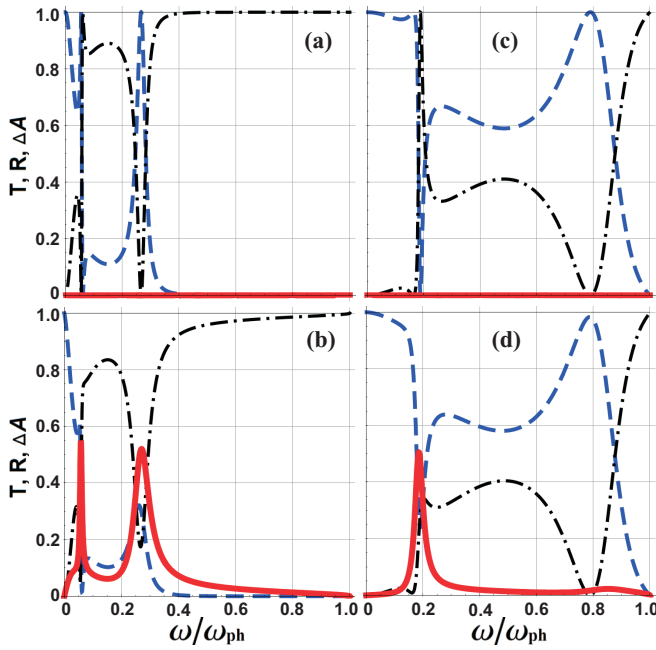
FIG. 6. Spectra of phonon energy transmission T (dashed line), reflection R (dotted-dashed line), and absorption ΔA (solid line) versus reduced frequency $\omega/\omega_{\text{ph}}$ at a checkerboard-type defect layer with parameters $m_2 = m$ and $\gamma_2 = \gamma$ for the cases: in (a) and (b) $\gamma_1 = 0.02\gamma$, $\gamma_{1*} = 0.14\gamma$ and impurity masses $m_1 = 3m$, $m_{1*} = m$ (intrinsic frequencies $\omega_1 \approx 0.0577\omega_{\text{ph}}$ and $\omega_{1*} \approx 0.265\omega_{\text{ph}}$), (a) without dissipation and (b) with dissipative parameters $\gamma_1' = 0.001\gamma$, $\gamma_{1*}' = 0.014\gamma$; in (c) and (d) $\gamma_1 = \gamma/15$, $\gamma_{1*} = \gamma$, impurity masses $m_1 = m_{1*} = m$ (intrinsic frequencies $\omega_1 \approx 0.183\omega_{\text{ph}}$ and $\omega_{1*} \approx 0.71\omega_{\text{ph}}$), (c) without dissipation and (d) with dissipative parameters $\gamma_1' = \gamma/150$ and $\gamma_{1*}' = 0.001\gamma$.

the CB model are the host atoms with $m_2 = m$ and $\gamma_2 = \gamma$, see Fig. 1 and the beginning of Sec. III A).

As for the minor total transmission frequency ω_{T1} (24), it fits the inequality $\omega_{T1} \lesssim \omega_1 \lesssim \omega_R$ at $\omega_R - \omega_{T1} \backsim (\gamma_1/\gamma)\omega_1 \ll \omega_1$. The resonance frequency (24) depends on the force constant γ_1 and the defect mass m_1 through the intrinsic frequency ω_1 [due to definition (13)]. From formulas (24) and (25) it follows that synchronization between the motion of the atoms in the defect plane and the motion of their neighboring host atoms occurs in such a way that at the low total transmission frequency the energy flux goes mainly through the channel with weakly bound and not-too-heavy impurities whereas at the high total transmission frequency the flux is transmitted mainly through the host atoms in the defect plane.

It turns out and will be shown below that the model of such type [its scattering spectra are displayed in Fig. 6(c)] differs radically from that with the heavy impurities [Fig. 2(a)] in the degree of tolerance for the inclusion of weak dissipation. By Eqs. (5) and (6) it follows that the displacement amplitudes u_0 and u_{0*} of the impurities m_1 and m_{1*}, respectively, obey the relations (cf. Ref. [40]):

$$\left(\omega^2 - \omega_1^2\right)u_0 = 0.5\omega_1^2\left(u_1^{(+)} + u_1^{(-)}\right),$$
$$\left(\omega^2 - \omega_{1*}^2\right)u_{0*} = 0.5\omega_{1*}^2\left(u_1^{(+)} + u_1^{(-)}\right), \qquad (26)$$

where $u_1^{(+)}$ and $u_1^{(-)}$ are the amplitudes of the displacements of the atoms in planes $p_3 = 1$ and $p_3 = -1$, respectively. If $\omega = \omega_1$, then from Eqs. (26) it follows that $u_1^{(+)} + u_1^{(-)} = 0$, and hence, $u_{0*} = 0$. It means that due to interference a phonon path through the impurities with masses m_{1*} is blocked. Similarly, at the frequency $\omega = \omega_{1*}$ the energy flux via the atoms with m_1 goes to zero.

According to Eqs. (26), the displacement amplitudes u_0 and u_{0*} are of the same sign at the low frequencies $\omega < \omega_1$ and at the high frequencies $\omega > \omega_{1*}$ if an inequality $\omega_1 < \omega_{1*} < \omega_{\text{ph}}$ takes place. In the intermediate phonon frequency domain $\omega_1 < \omega < \omega_{1*}$ the amplitudes u_0 and u_{0*} are of different signs; heterogeneous atoms in the defect plane fulfill antiphase oscillations. Just at the same frequency domain the total phonon reflection occurs as soon as the frequency ω_R from Eq. (21) is reached.

Stability of the solution (15)–(20) mathematically may be disturbed at the condition $\omega_T = \omega_R$. But substitution of $\omega = \omega_R$ from Eq. (21) into Eq. (23) leads to a conclusion that at $\gamma > \bar{\gamma} = (\gamma_1 + \gamma_{1*})/2$ total reflection frequency ω_R may be equal to total transmission frequency ω_T only when $\omega_1 = \omega_{1*}$. At this equality, in view of Eqs. (26), for all incident wave frequencies ω and for all defect atoms the displacement amplitudes are of the same value $u_0 = u_{0*}$, while the energy fluxes through each of both channels differ from each other. In this case, the destructive interference (transmission antiresonance) is absent. The defect plane scatters phonons similar to a homogeneous monoatomic layer with intrinsic frequency ω_1 and effective defect nearest-neighbor bond $\bar{\gamma}$. Therewith, the square of total transmission frequency ω_T^2 is

$$\omega_T^2 = \frac{\omega_1^2(2\gamma - \bar{\gamma}) - \omega_{\text{ph}}^2\bar{\gamma}^2/2\gamma}{2(\gamma - \bar{\gamma})}. \qquad (27)$$

It is implied that in Eq. (27) the existence condition $0 < \omega_T^2 < \omega_{\text{ph}}^2$ for ω_T is satisfied.

Evidently, there is an infinitely large number of checkerboard-type systems with equal parameters ω_1 and $\bar{\gamma}$, such as $\omega_1 = \omega_{1*} < \omega_{\text{ph}}$ and $\gamma > \bar{\gamma}$, and with a total transmission frequency, defined by Eq. (27). Any small variation of any one of four material parameters leads to the rise of another intrinsic frequency ω_{1*} in the vicinity of ω_1 (or ω_1 in the vicinity of ω_{1*}) and, in view of Eq. (22), produces at once destructive antiresonance ω_R as well as a new transmission resonance ω_T close to ω_R, i.e., $\omega_R \approx \omega_T$. The resulting type of phonon spectrum is independent of such variations, that is, two total transmission frequencies are separated by the total reflection frequency. This is a distinctive feature of the CB model as compared to the three-layer model studied further in Sec. IV.

At different values of the intrinsic frequencies and force constants the biquadratic equation (23) for constructive resonances may possess either one or two or no roots. When the conditions $\gamma > \bar{\gamma}$ and $\omega_1 < \omega_{1*} < \omega_{\text{ph}}$ are fulfilled, sets of parameters γ_1, γ_{1*}, ω_1, and ω_{1*} exist at which the total reflection frequency lies in the range between two total transmission frequencies. For example, below in Sec. III B as an analog of doubly resonant electromagnetic system we will discuss a case of the CB model with both defect masses equal (or almost equal) to the double mass m of the host atom, i.e.,

$m_1 = m_{1*} = 2m$ [see Fig. 4(a)]; the defect elastic constants are chosen to be $\gamma_1 = 0.14\gamma$ and $\gamma_{1*} = 0.4\gamma$ (the intrinsic frequencies $\omega_1 \approx 0.187\omega_{\text{ph}}$ and $\omega_{1*} \approx 0.316\omega_{\text{ph}}$). In this case the plane wave scattering reveals three strongly marked resonances: The minor total transmission frequency (resonance) and the total reflection frequency (antiresonance) are in the vicinity of the minor intrinsic frequency ($\omega_{T1} \lesssim \omega_1 \lesssim \omega_R$). The second total transmission frequency (resonance) is in the vicinity of the major intrinsic frequency $\omega_{T2} \approx \omega_{1*}$ ($\omega_R < \omega_{T2}$), so a well-defined narrow antiresonance transmission dip and two more wide pass bands take place in the phonon transmission spectrum. From Fig. 4(a) one can draw a conclusion that in the CB model a low intrinsic frequency in the weak-binding approximation for defect atoms is resonant for increasing forward scattering provided that the corresponding weak-binding transmission channel is the more powerful of the two, whereas at a minor intrinsic frequency the total phonon reflection (antiresonance) is observed.

Another option of the same pattern with $\gamma > \bar{\gamma}$ and $m_1 = m_{1*} = 2m$ is depicted in Fig. 3(a) with parameters $\gamma_1 = 0.14\gamma$ and $\gamma_{1*} = 1.8\gamma$. There is a very narrow terahertz-frequency transmission antiresonance ($\omega_R \approx 0.1936\omega_{\text{ph}}$) against the background of a very wide frequency pass band. A system with such destructive interference dip in the phonon spectrum may be used as metafilter or metamirror there required. It should be noted that high-frequency scattering properties in this case are totally unlike those presented in Fig. 4(a) where a wide high-frequency range of almost total nontransmission exists.

B. Double-humped phonon absorption by checkerboard-type defect monolayer

It is well known [78] that attenuation can significantly change the behavior of a system in the vicinity of resonance frequencies. In the nondissipative limit the incident wave energy is radiated into the crystal volume by reflected and transmitted waves. At finite dissipation, the energy localized near a defect hereafter travels into the bulk through the relaxation processes in the nonequilibrium heat carrier system. There exist different energy exchange channels connected with relaxation in the phonon system, for example, phonon-phonon scattering, phonon interaction with conduction electrons in metals, phonon scattering by the crystal boundaries in monocrystals and polycrystals, scattering in the surface area by the asperities, scattering by impurities, scattering by crystal defects.

In the general model (Fig. 1), the relatively weak dissipation in the defect interior is assumed to be predominant over the rest of energy exchange mechanisms. So, an influence of inner dissipative processes on the interaction of the incident wave with defect layer is studied under the assumption that after the energy accumulation in the defect area the heat transport to the surrounding medium is determined by scattering processes of a higher approximation than is discussed here.

Following a conventional phenomenological technique (see, e.g., Ref. [78] for more details), the dissipative function which gives the rate of energy dissipation in the system is introduced. Further, all generalized frictional forces in the volume of a bulk crystal are supposed to be small in contrast

with those in the defect layer. It is well known that the small friction taken into account in the first approximation of the perturbation theory gives a small imaginary contribution in the vibration frequencies, corresponding to oscillation damping in time. Appearance of such contribution may be provided by adding a small imaginary component in the force constants (see, e.g., Ref. [80]).

In this section the effect of attenuation of defect layer oscillations on the phonon multipath interference reflection and transmission is analyzed in such a case of the CB model that can be considered as an analog of the doubly resonant electromagnetic system. To introduce the energy absorption losses of these oscillations into the pattern of calculation one has to replace the real force constants γ_i ($i = 1, 1*$) in Eqs. (15)–(20) by the complex values $\gamma_i \rightarrow \gamma_i - i\gamma_i'$ and the intrinsic frequencies ω_1 and ω_{1*} in Eq. (13) by the complex values:

$$\omega_i^2 \rightarrow \omega_i^2(1 - i\gamma_i'/\gamma_i), \quad i = 1, 1*. \tag{28}$$

Here both imaginary parts are positive, $\gamma_i' > 0$, and for simplicity taken to be frequency independent.

One can calculate the absorption by the checkerboard-type defect layer as

$$\Delta A = 1 - |a_R|^2 - |a_T|^2. \tag{29}$$

Assuming that $\gamma_i \gg \gamma_i'$, the value ΔA in Eq. (29) may be presented approximately as the sum of three terms:

$$\Delta A \approx \Delta A_2 + \Delta A_1 + \Delta A_{1*}, \tag{30}$$

where the values ΔA_i at $i = 1, 1*$ account for the viscous motions of the impurities with the masses m_1 and m_{1*}, correspondingly,

$$\Delta A_i = \frac{\gamma_i' \omega_{\text{ph}}^2 \sqrt{\omega_{\text{ph}}^2 - \omega^2} \, \omega^3 (\omega^2 - \omega_j^2)^2}{2\gamma |D_{\text{CB}}(\omega)|^2}, \tag{31}$$

(here $j = 1*$ at $i = 1$ and $j = 1$ at $i = 1*$), and ΔA_2 is the energy losses due to viscous motion of the boundary planes $p = \pm 1$:

$$\Delta A_2 = \frac{32\gamma\omega\sqrt{\omega_{\text{ph}}^2 - \omega^2}(\gamma_1' + \gamma_{1*}')}{\omega_{\text{ph}}^2 |4\gamma \exp(ik) - B_{\text{CB}}^{(-)}|^2}. \tag{32}$$

In Eqs. (31) and (32) the values $B_{\text{CB}}^{(-)}$ and $D_{\text{CB}}(\omega)$ are defined by Eqs. (19) and (20) with complex values of the force constants and intrinsic frequencies. As one would expect, $\Delta A_i = 0$ ($i = 1, 1*$) at the same frequency ω_j ($j = 1*, 1$) when the phonon transmission channel, marked off by index i, is blocked in the nondissipative case (see Sec. III A).

For a checkerboard-type defect layer the coefficients of phonon energy transmission $T(\omega)$ and reflection $R(\omega)$ as well as interface phonon energy absorption $\Delta A(\omega)$ versus reduced frequency ω are shown in Figs. 4 and 5 with the following parameters: impurity masses $m_1 = m_{1*} = 2m$ and elastic force constants $\gamma_1 = 0.14\gamma$, $\gamma_{1*} = 0.4\gamma$. The results of exact calculations from the formula (29) with Eqs. (15)–(20) are presented in Fig. 4 for the cases: (a) in the absence of dissipation $\gamma_1' = \gamma_{1*}' = 0$, $\Delta A = 0$; (b) $\gamma_1' = 0.012\gamma$, $\gamma_{1*}' = 0.1\gamma$; (c) $\gamma_1' = 0.006\gamma$, $\gamma_{1*}' = 0.09\gamma$; (d) $\gamma_1' = 0.02\gamma$, $\gamma_{1*}' = 0.02\gamma$. Analogous exact calculations with $\gamma_1' = 0.02\gamma$ and

$\gamma'_{1*} = 0.04\gamma$ are depicted in Fig. 5(a) and interface absorption computed with the approximate formulas (30), (31), and (32) is presented in Fig. 5(b) for the same system as in Fig. 5(a). The close agreement of the exact [Fig. 5(a)] and the approximate [Fig. 5(b)] results allows us to accept the latter as correct.

One can see that the double-humped surface energy absorption curves in Figs. 4(b), 4(c), 4(d), and 5(a) with different values of weak dissipative parameters are similar to the transmission cross section spectra of a double-slit structure in a perfect electric conductor film with different angles of wave incidence [32]. Moreover, the approximate locations of ω_{max1} and ω_{max2}, where absorption reaches its peaks, for the cases in Figs. 4 and 5 are independent of the local viscous dissipation like in Ref. [32], where the position of the narrow resonance relative to the broad resonance remains approximately unchanged as the angle of incidence is varied.

The approximate values of ω_{max1}^2 and ω_{max2}^2 for the cases illustrated in Figs. 4 and 5 are equal to:

$$\omega_{max1}^2 \simeq \omega_1^2 + \frac{\gamma_1 \omega_{ph}^2}{4\gamma(\omega_{ph}^2 - \omega_1^2)}\left[\omega_1^2 + \omega_{ph}^2\frac{\gamma_1(\omega_{ph}^2 - 2\omega_1^2)}{16\gamma(\omega_{ph}^2 - \omega_1^2)}\right.$$
$$\left. + \omega_{ph}^2\frac{\gamma_{1*}\omega_1^2}{4\gamma(\omega_{1*}^2 - \omega_1^2)}\right] \qquad (33)$$

and

$$\omega_{max2}^2 \simeq \omega_{1*}^2 + \frac{\gamma_{1*}\omega_{ph}^2}{4\gamma(\omega_{ph}^2 - \omega_{1*}^2)}\left[\omega_{1*}^2 + \omega_{ph}^2\frac{\gamma_{1*}(\omega_{ph}^2 - 2\omega_{1*}^2)}{16\gamma(\omega_{ph}^2 - \omega_{1*}^2)}\right.$$
$$\left. + \omega_{ph}^2\frac{\gamma_1\omega_{1*}^2}{4\gamma(\omega_1^2 - \omega_{1*}^2)}\right]. \qquad (34)$$

For specific cases in Figs. 4 and 5, the squares of intrinsic frequencies $\omega_1^2 = 0.035\omega_{ph}^2$ and $\omega_{1*}^2 = 0.1\omega_{ph}^2$ may be used for obtaining from Eqs. (33) and (34) the approximate numerical values $\omega_{max1} \approx 0.196\omega_{ph}$ and $\omega_{max2} \approx 0.328\omega_{ph}$.

The minimum absorption frequency ω_{min} between ω_{max1} and ω_{max2} in Fig. 5 is located almost in the intersection of lines $\Delta A_1(\omega)$ and $\Delta A_{1*}(\omega)$. For this case $\omega_1 < \omega_{min} < \omega_{1*}$, and we arrive at the approximate analytical formula

$$\omega_{min}^2 \simeq \frac{\omega_{1*}^2\sqrt{\gamma'_1} + \omega_1^2\sqrt{\gamma'_{1*}}}{\sqrt{\gamma'_1} + \sqrt{\gamma'_{1*}}} \qquad (35)$$

and further, from Eq. (35) at the corresponding numerical value $\omega_{min} \simeq 0.249\omega_{ph}$.

The broad peak height $\Delta A(\omega_{max2})$ may be found approximately as

$$\Delta A(\omega_{max2}) \simeq \Delta A_{1*}(\omega_{1*}) + \Delta A_2(\omega_{1*}), \qquad (36)$$

where the first term is

$$\Delta A_{1*}(\omega_{1*}) \simeq \frac{8\gamma\gamma'_{1*}\omega_{1*}\sqrt{\omega_{ph}^2 - \omega_{1*}^2}}{8\gamma\gamma'_{1*}\omega_{1*}\sqrt{\omega_{ph}^2 - \omega_{1*}^2} + \omega_{ph}^2\gamma_{1*}^2} \qquad (37)$$

and the second term is

$$\Delta A_2(\omega_{1*}) \simeq 8\gamma(\gamma'_1 + \gamma'_{1*})\omega_{1*}\sqrt{\omega_{ph}^2 - \omega_{1*}^2}\big[8\gamma(\gamma'_1$$
$$+ \gamma'_{1*})\omega_{1*}\sqrt{\omega_{ph}^2 - \omega_{1*}^2} + \omega_{ph}^2(\gamma_1 + \gamma_{1*})^2$$
$$+ 8\omega_{1*}^2\gamma(2\gamma - \gamma_1 - \gamma_{1*})\big]^{-1}. \qquad (38)$$

These formulas yield a good agreement between the approximate numerical value $\Delta A(\omega_{max2}) \simeq 0.4648$ in Fig. 4(b) and the exact value in Fig. 5(a).

The height of the narrow peak $\Delta A(\omega_{max1})$ may be estimated as

$$\Delta A(\omega_{max1}) \simeq \Delta A_1(\omega_{max1}) + \Delta A_2(\omega_{max1}). \qquad (39)$$

The second term $\Delta A_2(\omega_{max1})$ in Eq. (39), accounting for the absorption contribution of the boundary layers, may be calculated as $\Delta A_2(\omega_{max1}) \simeq \Delta A_2(\omega_1)$ and is obtained from Eq. (38) after replacing ω_{1*} by ω_1:

$$\Delta A_2(\omega_1) \simeq 8\gamma(\gamma'_1 + \gamma'_{1*})\omega_1\sqrt{\omega_{ph}^2 - \omega_1^2}\big[8\gamma(\gamma'_1$$
$$+ \gamma'_{1*})\omega_1\sqrt{\omega_{ph}^2 - \omega_1^2} + \omega_{ph}^2(\gamma_1 + \gamma_{1*})^2$$
$$+ 8\omega_1^2\gamma(2\gamma - \gamma_1 - \gamma_{1*})\big]^{-1}. \qquad (40)$$

To get a good agreement of the term $\Delta A_1(\omega_{max1})$ in Eq. (39) with the exact value it is necessary to use Eq. (33) for calculation of ω_{max1}, and then the obtained result has to be substituted into Eq. (31) at $i = 1$. As a consequence of the above calculations, the approximate narrow peak height is found to be $\Delta A_1(\omega_{max1}) \simeq 0.59$. This value is very close to the true one in Fig. 5(a) and the approximate one in Fig. 5(b).

In the vicinity of the frequency ω_{max2} the term $\Delta A_{1*}(\omega)$ in formula (30) is expressed by a Lorentzian

$$\Delta A_{1*}(\omega \sim \omega_{max2}) \simeq \frac{\Delta A_{1*}(\omega_{max2})}{1 + \tau_2^2(\omega - \omega_{max2})^2} \qquad (41)$$

with τ_2^2 from

$$\tau_2^2 = \frac{32\gamma}{\gamma_{1*}^2\omega_{ph}^2 + 8\gamma'_{1*}\gamma\omega_{1*}\sqrt{\omega_{ph}^2 - \omega_{1*}^2}}\left\{2\gamma - 3\gamma_{1*} - \gamma_1 + \frac{\omega_1^2(2\gamma_{1*} + \gamma_1)}{\omega_1^2 - \omega_{1*}^2} + \omega_{ph}^2\frac{2\omega_{1*}^4(\gamma_{1*} + \gamma_1)^2 - (\gamma_{1*}\omega_1^2 + \gamma_1\omega_{1*}^2)^2}{8\gamma\omega_{1*}^2(\omega_1^2 - \omega_{1*}^2)^2}\right.$$
$$\left. + \frac{\gamma_{1*}^2}{8\gamma}\left[\frac{\omega_{ph}^2(3\omega_{ph}^2 - 4\omega_{1*}^2)}{(\omega_{ph}^2 - \omega_{1*}^2)(\omega_1^2 - \omega_{1*}^2)} - \frac{\omega_{ph}^2\omega_{1*}^2}{(\omega_1^2 - \omega_{1*}^2)^2} + \frac{\omega_{ph}^4(5\omega_{ph}^2 - 4\omega_{1*}^2)}{8\omega_{1*}^2(\omega_{ph}^2 - \omega_{1*}^2)^2}\right] + \frac{\gamma'_1\omega_{1*}^3\sqrt{\omega_{ph}^2 - \omega_{1*}^2}}{(\omega_1^2 - \omega_{1*}^2)^2}\right\}. \qquad (42)$$

In the vicinity of the frequency ω_{max1} the term $\Delta A_1(\omega)$ in formula (30) is expressed by another Lorentzian

$$\Delta A_1(\omega \sim \omega_{max1}) \simeq \frac{\Delta A_1(\omega_{max1})}{1 + \tau_1^2(\omega - \omega_{max1})^2} \qquad (43)$$

with τ_1^2 from

$$\tau_1^2 = \frac{32\gamma}{\gamma_1^2\omega_{\mathrm{ph}}^2 + 8\gamma_1'\gamma\omega_1\sqrt{\omega_{\mathrm{ph}}^2 - \omega_1^2}}\left\{2\gamma - 3\gamma_1 - \gamma_{1*} + \frac{\omega_{1*}^2(2\gamma_1 + \gamma_{1*})}{\omega_{1*}^2 - \omega_1^2} + \omega_{\mathrm{ph}}^2\frac{2\omega_1^4(\gamma_1 + \gamma_{1*})^2 - (\gamma_1\omega_{1*}^2 + \gamma_{1*}\omega_1^2)^2}{8\gamma\omega_1^2(\omega_{1*}^2 - \omega_1^2)^2}\right.$$

$$\left. + \frac{\gamma_1^2}{8\gamma}\left[\frac{\omega_{\mathrm{ph}}^2(3\omega_{\mathrm{ph}}^2 - 4\omega_1^2)}{(\omega_{\mathrm{ph}}^2 - \omega_1^2)(\omega_{1*}^2 - \omega_1^2)} - \frac{\omega_{\mathrm{ph}}^2\omega_1^2}{(\omega_{1*}^2 - \omega_1^2)^2} + \frac{\omega_{\mathrm{ph}}^4(5\omega_{\mathrm{ph}}^2 - 4\omega_1^2)}{8\omega_1^2(\omega_{\mathrm{ph}}^2 - \omega_1^2)^2}\right] + \frac{\gamma_1'\omega_1^3\sqrt{\omega_{\mathrm{ph}}^2 - \omega_1^2}}{(\omega_{1*}^2 - \omega_1^2)^2}\right\}. \tag{44}$$

In Fig. 5 the narrow peak width τ_1^{-1} in view of Eq. (44) depends on γ_1' and is almost independent of γ_{1*}'. As γ_{1*}' increases, then the γ_{1*}' dependence of τ_1 becomes noticeable. A decrease of γ_1' or an increase of γ_{1*}' make the value τ_1 greater and the width of the narrow peak smaller. The broad peak width τ_2^{-1} depends also on γ_1' and γ_{1*}' but in another way: The broad peak gets narrower as γ_1' increases or γ_{1*}' decreases in view of Eq. (42). The Lorentzian interface absorption approximations by Eqs. (41) and (43) are also similar to the behavior of the transmission cross section spectra of the electromagnetic doubly resonant structure described in Ref. [32].

The case considered above is one of the more representative types of the CB model. Its essential feature is that the total reflection frequency and one of the total transmission frequencies are fairly close together in the nondissipative limit. If the weak dissipation is allowed for, this peculiarity results in a spectrum of the interface energy absorption where the narrow peak, placed against the background of the broad hump, is shifted to the lower frequencies from the broad hump maximum. This case may be of essential interest for investigations of the thermal interface resistance as well as the other options, shown in Figs. 6 and 7 (see also Ref. [79]).

One can see that a necessary condition for occurrence of two peaks in the energy absorption at the two-path phonon interference is the existence of two total transmission phonon frequencies within corresponding phonon spectrum in the nondissipative limit [see Figs. 6(a) and 7(a)]. An absorption peak may be very sharp if the total transmission and total reflection frequencies (without losses) are located very close to each other (see Figs. 6 and 7) or if in the vicinity of the total transmission frequency the scattering coefficient $T(\omega)$ changes abruptly with frequency, showing the narrow peak [Fig. 6(a)]. But double-peaked absorption resonance is not necessarily the case for the systems with two nondissipative total transmission phonon frequencies. For example, in Fig. 6(c) there are two total transmission frequencies, however there is only one domain with narrow limits wherein the corresponding absorption phonon spectrum peaks sharply [Fig. 6(d)]. Outside this domain the energy absorption is negligibly small.

For different sets of the defect parameters the resonance absorption peaks are different in height, width, and location. As defect parameters change, the narrow peak may die away when the broad peak becomes higher and its width becomes bigger or smaller. As a rule, in the CB model the narrow peak is to the left of the broad peak if either is located away from the Brillouin zone edge. In the vicinity of this boundary the broad peak may be narrow as in Fig. 7(b). If the major intrinsic
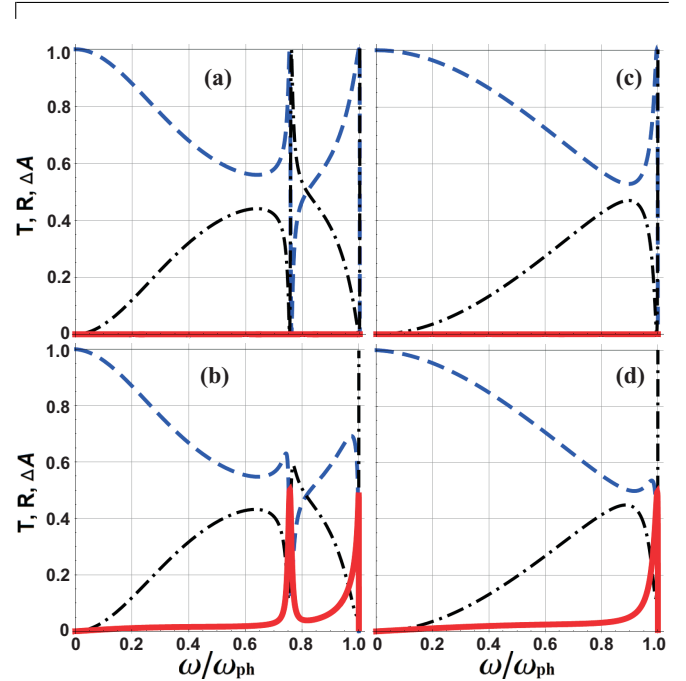

FIG. 7. Spectra of phonon energy transmission T (dashed line), reflection R (dotted-dashed line), and absorption ΔA (solid line) versus reduced frequency $\omega/\omega_{\mathrm{ph}}$ at a checkerboard-type defect layer with parameters $m_2 = m$ and $\gamma_2 = \gamma$ for the cases: in (a) and (b) $\gamma_1 = 0.2\gamma$, $\gamma_{1*} = \gamma$ and impurity masses $m_1 = 0.18m$, $m_{1*} = 0.7m$ (intrinsic frequencies $\omega_1 \approx 0.745\omega_{\mathrm{ph}}$ and $\omega_{1*} \approx 0.845\omega_{\mathrm{ph}}$), (a) without dissipation and (b) with dissipative parameters $\gamma_1' = \gamma/450$, $\gamma_{1*}' = 0.01\gamma$; in (c) and (d) $\gamma_1 = 0.81\gamma$, $\gamma_{1*} = 0.95\gamma$ and impurity masses $m_1 = 0.5m$, $m_{1*} = m/7$ (intrinsic frequencies $\omega_1 = 0.9\omega_{\mathrm{ph}}$ and $\omega_{1*} \approx 1.82\omega_{\mathrm{ph}}$), (c) without dissipation and (d) with dissipative parameters $\gamma_1' = 0.008\gamma$, $\gamma_{1*}' = 0.014\gamma$.

frequency is beyond the Brillouin zone edge, i.e., $\omega_{1*} > \omega_{\mathrm{ph}}$, only one absorption peak remains in the frequency domain $0 \leqslant \omega \leqslant \omega_{\mathrm{ph}}$ as in Fig. 7(d). But an attempt to achieve the total phonon energy absorption in the CB model fails due to its simple symmetry using only four defect parameters, in contrast with the triple-defect-layer model discussed below in Sec. IV.

The simple symmetry of the checkerboard-type model reveals itself also at the equality of the intrinsic frequencies $\omega_1 = \omega_{1*}$. As in the lossless case, discussed previously in Sec. III A, at weak dissipation taken into account, the defect plane moves as if only one phonon path to propagate existed. In this case only one noticeable peak in interface phonon absorption may be observed, much as illustrated below in Fig. 16. While its height does not reach point 1, this

peculiarity in the interface absorption can effect on the heat transfer through such a planar defect.

It should be mentioned that in the general case the absorption peak locations fall on neither the intrinsic frequencies nor the total transmission frequencies nor the total reflection frequency in the nondissipative limit because of resulting complex collective dynamic motion. For the problem of the thermal interface resistance it is important that the following peculiarities due to weak dissipation should be taken into account. If in the lossless limit the frequency dependence of the scattering coefficients is fairly monotonous, then in the respective dissipative cases and corresponding frequency domains the interface absorption is very small (see Figs. 6 and 7). Moreover, if back scattering or forward scattering is vanishingly small it will be almost so in a dissipative system. The energy of the other flux is reduced by the phonon interface energy absorption. In particular, this is true for total transmission and total reflection frequencies displayed, for example, in Fig. 2 [see also Figs. 6(c) and 6(d)] for Ar metamaterial with the planar defect filled by Ar and its heavy isotopes in checker order, i.e., for a system discussed above in Sec. III A. Figures 2(b) and 6(d) illustrate that the scattering resonance frequencies in dissipative systems exist and may be identified by disappearance of the corresponding fairly monotone scattering coefficient: A lossless total phonon transmission transforms into an almost total dissipative nonreflection and, vice versa, a lossless total phonon reflection becomes an almost total dissipative nontransmission.

IV. RESONANCE PHONON ABSORPTION BY TWO-DIMENSIONAL TRIPLE DEFECT LAYER (TL MODEL)

The objective of this section is to consider another simple option of the general model (Fig. 1), in which two-path phonon interference reveals itself as total phonon transmission and total phonon reflection in the lossless limit and as double-humped (double-peaked) resonance in the phonon interface absorption at weak dissipation taken into account. This is the TL model which contains a defect layer composed of three impurity atomic planes. Two outer identical monolayers ($p_3 = \pm 1$) with impurity masses m_2 interact directly through the next-to-nearest-neighbor bond γ_3. They are adjacent to the opposite host crystal semispaces and bound, firstly, by the nearest-neighbor bond γ_2 to the host atoms in the planes $p_3 = \pm 2$ and, secondly, by the nearest-neighbor bond γ_1 with an inner defect layer $p_3 = 0$, fully occupied by impurities with masses m_1 [see Eqs. (1)–(8) and Fig. 1 at $\gamma_1 = \gamma_{1*}$ and $m_1 = m_{1*}$]. In the TL model two paths exist for phonons to penetrate the defect layer: Through the interatomic bonds γ_1 and masses m_1 and through direct interatomic bonds γ_3, bypassing the intermediate impurity atomic plane.

Using all above-listed criteria in Eqs. (10)–(12), restricting present consideration to the case of normal phonon incidence, for the reflection and transmission amplitudes $a_R(\omega)$ and $a_T(\omega)$ it is easy to obtain such expressions:

$$a_R(\omega) = \frac{\exp(-4ik)}{D(\omega)} \frac{\omega}{2\omega_2^4} \{8\gamma_2^2\gamma^2\omega_2^4(\omega^2 - \omega_1^2) + [2\gamma_2(\omega_1^2 - \omega^2) + \gamma_1\omega_2^2][\gamma_2^2\omega_{ph}^2 - 4\gamma(\gamma_2 - \gamma)\omega^2]$$

$$\times [(2\gamma_1 + \gamma_3)\omega_2^2 - 4\gamma_2\omega^2] + 2\gamma\gamma_2(2\gamma - \gamma_2)\omega_2^2$$

$$\times [2\gamma_1\omega_1^2\omega_2^2 - (8\gamma_2\omega^2$$

$$-4\gamma_1\omega_2^2 - \gamma_3\omega_2^2)(\omega^2 - \omega_1^2)]\}, \tag{45}$$

$$a_T(\omega) = i\frac{\exp(-4ik)}{D(\omega)}\gamma\gamma_2^2\gamma_3\sqrt{\omega_{ph}^2 - \omega^2}(\omega_R^2 - \omega^2), \tag{46}$$

where

$$D(\omega) = \frac{1}{\omega_{ph}^2\omega_2^4}\Big\{2\gamma\big(\omega + i\sqrt{\omega_{ph}^2 - \omega^2}\big)\big[\gamma_2\big(2\omega^2 - \omega_2^2\big)\big(\omega^2$$

$$-\omega_1^2\big) - \gamma_1\omega_2^2\omega^2\big] - \gamma_2\omega\omega_{ph}^2\big[2\gamma_2\big(\omega^2 - \omega_1^2\big)$$

$$-\gamma_1\omega_2^2\big]\Big\}\Big\{\gamma_2^2\omega_2^2\omega_{ph}^2 + \Big[\gamma\omega\big(\omega + i\sqrt{\omega_{ph}^2 - \omega^2}\big)$$

$$-\frac{\gamma_2}{2}\omega_{ph}^2\Big]\big[2\gamma_2\big(\omega_2^2 - 2\omega^2\big) + (2\gamma_1 + \gamma_3)\omega_2^2\big]\Big\}, \tag{47}$$

and ω_2 denotes an intrinsic frequency:

$$\omega_2 = 2\sqrt{2\gamma_2/m_2}. \tag{48}$$

In Eq. (46) the total reflection frequency ω_R, obtained from Eq. (14), is given by the expression:

$$\omega_R = \omega_1\sqrt{1 + \frac{2\gamma_1}{\gamma_3}}. \tag{49}$$

In Eqs. (45)–(49) the values γ_1, γ_2, and γ_3 are real in the nondissipative limit, which is to say that we neglect attenuation of impurity vibrations.

First of all, it should be pointed out that the phonon scattering spectrum of the nondissipative TL model may include three total transmission frequencies ω_T, which are the roots of the bicubic equation in the numerator of Eq. (45) for the reflection amplitude $a_R(\omega)$. This feature is due to such description of the system that uses five material parameters and, consequently, corresponds to the collective dynamic motion more complicated than in the CB model. In what follows, the peculiarities of the phonon scattering by the triple defect layer, arising from its specific parametrization, are described. If only two frequencies ω_T exist, then both of them may lie on one side of the total reflection frequency ω_R. For example, for different sets of parameters, it can be seen in Fig. 8(a) that two total transmission frequencies are to the right of the frequency ω_R and in Figs. 8(c) and 9(a) they are to its left (see also Figs. 8 and 9 in Ref. [79] for more detail). Below it will be shown that in this model the material parameters at which the frequency ω_T coincides with the frequency ω_R exist only if the dissipation is allowed for. Without considering attenuation, an attempt to find such parameters that the distance between frequencies ω_R and ω_T is ultimately reduced, originates situations depicted in Figs. 10(a) and 11(a). In Fig. 10(a) two transmission maxima on either side of the total reflection frequency in its vicinity are smaller than 1. In Fig. 11(a) a special case with only one total transmission frequency ω_T is presented.

To study the interface phonon absorption in the TL model, a coefficient of phonon energy absorption $\Gamma_i(\omega)$ ($i = 1, 3$) is introduced for the channel numbered i. The value of $\Gamma_i^{-1}(\omega)$ is the time it takes for the intensity of oscillations with frequency
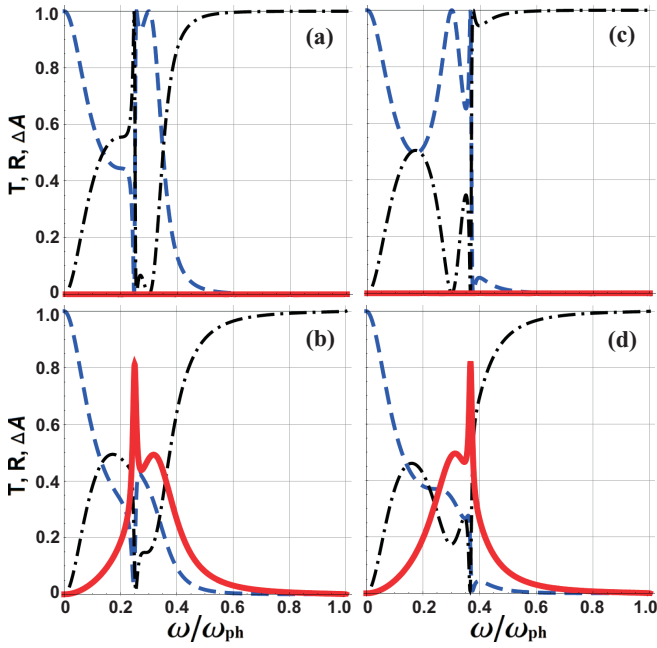
FIG. 8. Spectra of phonon energy transmission T (dashed line), reflection R (dotted-dashed line), and absorption ΔA (solid line) versus reduced frequency $\omega/\omega_{\mathrm{ph}}$ at a triple defect layer with parameter $\gamma_2 = 1.1\gamma$, impurity masses $m_1 = 0.8m$ and $m_2 = 5m$ for the cases: in (a) and (b) elastic constants $\gamma_3 = 3.6\gamma$, $\gamma_1 = 0.093\gamma$, in (c) and (d) elastic constants $\gamma_3 = 3.2\gamma$ and $\gamma_1 = 0.2\gamma$; (a) and (c) without dissipation; (b) and (d) with dissipative parameters $\gamma_3' = 0.446\gamma\omega\omega_{\mathrm{ph}}/(\omega^2 + \omega_{\mathrm{ph}}^2/16)$, $\gamma_1' = 0.0014\gamma\omega\omega_{\mathrm{ph}}/(\omega^2 + \omega_{\mathrm{ph}}^2/16)$.

ω in i-cannel to decrease by the factor e. By analogy with macroscopic "dissipative acoustic theory" (see, for example, Ref. [80]), the elastic force constant γ_1 is to be multiplied by the value $(1 - i\omega\Gamma_1(\omega)/\omega_1^2)$, which implies replacing γ_1 in the expressions (45)–(49) for the complex transmission and reflection amplitudes by the complex value $\gamma_1 \rightarrow \gamma_1 - i\gamma_1'$ with the imaginary part $\gamma_1' = \gamma_1\omega\Gamma_1(\omega)/\omega_1^2$. As for the initial bonding force γ_3, it is replaced by a complex value $\gamma_3 \rightarrow \gamma_3 - i\gamma_3'$
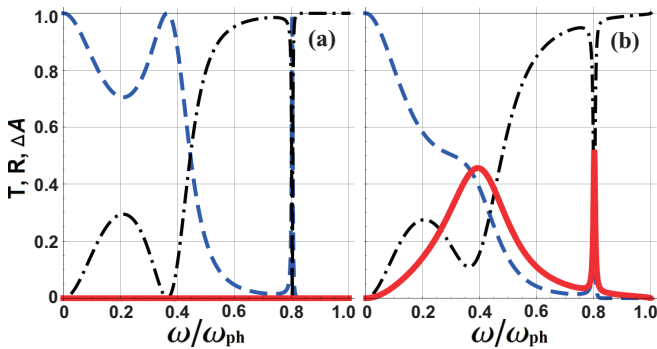

FIG. 9. Spectra of phonon energy transmission T (dashed line), reflection R (dotted-dashed line), and absorption ΔA (solid line) versus reduced frequency $\omega/\omega_{\mathrm{ph}}$ at a triple defect layer with parameter $\gamma_2 = 1.1\gamma$, impurity masses $m_1 = 0.16m$ and $m_2 = 3.2m$, elastic constants $\gamma_3 = 3.2\gamma$ and $\gamma_1 = 0.2\gamma$ for the cases: (a) without dissipation; (b) with dissipative parameters $\gamma_3' = 0.446\gamma\omega\omega_{\mathrm{ph}}/(\omega^2 + \omega_{\mathrm{ph}}^2/16)$, $\gamma_1' = 0.00075\gamma\omega\omega_{\mathrm{ph}}/(\omega^2 + \omega_{\mathrm{ph}}^2/16)$.
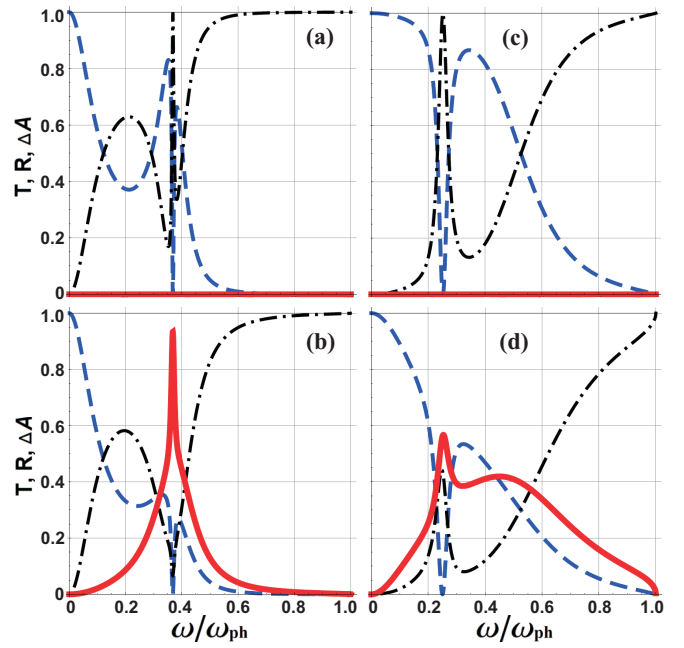

FIG. 10. Spectra of phonon energy transmission T (dashed line), reflection R (dotted-dashed line), and absorption ΔA (solid line) versus reduced frequency $\omega/\omega_{\mathrm{ph}}$ at a triple defect layer with parameter $\gamma_2 = 1.1\gamma$, impurity mass $m_1 = 0.8m$ for the cases: in (a) and (b) $m_2 = 5m$, $\gamma_1 = 0.2\gamma$, $\gamma_3 = 4.8\gamma$; in (c) and (d) $m_2 = 1.5m$, $\gamma_1 = 0.093\gamma$, $\gamma_3 = 2.08\gamma$; (a) and (c) without dissipation; (b) and (d) with dissipative parameters $\gamma_1' = 0.0014\gamma\omega\omega_{\mathrm{ph}}/(\omega^2 + \omega_{\mathrm{ph}}^2/16)$, $\gamma_3' = 0.446\gamma\omega\omega_{\mathrm{ph}}/(\omega^2 + \omega_{\mathrm{ph}}^2/16)$.

with the imaginary part γ_3' equal to $\gamma_3' = 8\gamma_2\omega\Gamma_3(\omega)/\omega_2^2 - 4\gamma_1'$.

Notice that in the simplest theory of forced oscillations under friction [78], the absorption has different nature at low and high frequencies of the external periodic force. In the first case, the mean amount of energy absorbed per unit time is almost independent of the frequency, provided that damping
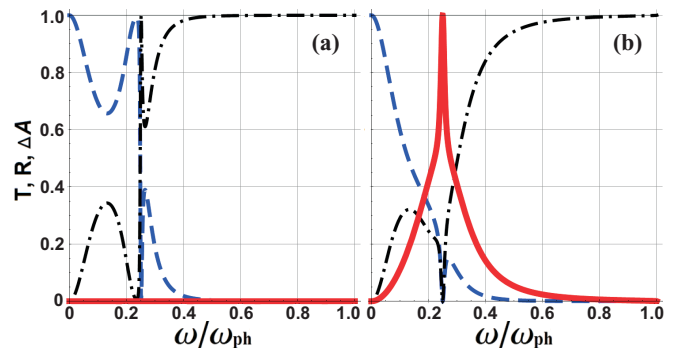

FIG. 11. Spectra of phonon energy transmission T (dashed line), reflection R (dotted-dashed line), and absorption ΔA (solid line) versus reduced frequency $\omega/\omega_{\mathrm{ph}}$ at a triple defect layer with parameters $\gamma_1 = 0.093\gamma$, $\gamma_2 = 1.1\gamma$, $\gamma_3 = 2.08\gamma$ and impurity masses $m_1 = 0.8m$, $m_2 = 5m$ for the cases: (a) without dissipation; (b) with dissipative parameters $\gamma_1' = 0.0014\gamma\omega\omega_{\mathrm{ph}}/(\omega^2 + \omega_{\mathrm{ph}}^2/16)$, $\gamma_3' = 0.466\gamma\omega\omega_{\mathrm{ph}}/(\omega^2 + \omega_{\mathrm{ph}}^2/16)$, anomalous total absorption $\Delta A(\omega_R) = 1$ is observed.

is realized through excitation of the exponentially decreasing eigenmodes. At high frequency the energy is continually absorbed by the system from an external source, dissipated by friction, and its mean value depends on the frequency. This steady motion is known as "dispersion-type frequency dependence of the absorption." To include in the present consideration the frequency dependence of $\Gamma_i(\omega)$ with both above limits, for example, the following approximation may be used:

$$\gamma_i'(\omega) = \Xi_{i0} \frac{\gamma \omega \omega_c}{\omega^2 + \omega_c^2}, \quad i = 1, 3, \quad (50)$$

where ω_c is the characteristic frequency above which the coefficients of phonon energy absorption $\Gamma_i(\omega)$ show frequency dispersion. The phonon damping is supposed to be weak and hence the dimensionless damping constants Ξ_{i0} are supposed to be small compared to 1, i.e., $\Xi_{i0} \ll 1$. The elastic forces of the medium γ and between the medium and triple defect layer γ_2 remain purely real.

In Figs. 8(b), 8(d), 9(b), 10(b), and 11(b) the frequency dependencies of the transmission coefficient $T(\omega) = |a_T|^2$, the reflection coefficient $R(\omega) = |a_R|^2$, as well as the interface absorption $\Delta A(\omega)$ calculated by the formula (29) with regard to weak dissipation in the triple defect layer, are shown in the systems answering the respective nondissipative cases presented in Figs. 8(a), 8(c), 9(a), 10(a), and 11(a). In the dissipative systems the imaginary contributions appear only in the parameters γ_3 and γ_1. For calculations the frequency ω_c is taken to be $\omega_c = \omega_{ph}/4$.

Figures 8(b), 8(d), 9(b) illustrate the cases of double-humped (double-peaked) phonon interface absorption in the TL model. If both of the total transmission frequencies ω_T are located on one side of the total reflection frequency ω_R, as in Figs. 8(a) and 8(c), then the narrow absorption peaks in Figs. 8(b) and 8(d), correspondingly, fall on the small frequency regions where one of the total transmission frequencies almost coincides with the total reflection frequency. In the dissipative systems at these frequencies reflected and transmitted energies drop both to their minima simultaneously. The narrow absorption peak may be located in the high frequency domain, as in Fig. 9(b), with a local minimum of the reflection coefficient only. Another absorption maximum of the broad peak is shifted to the frequency domain between the second transmission frequency and the frequency of the most abrupt jump of the nondissipative transmission and reflection coefficients where the most intensive energy redistribution between transmitted and reflected waves occurs [see Figs. 8(b), 8(d), and 9(b)].

A situation is possible where instead of two total transmission maxima there will be two local transmission maxima which will be located on the different sides of the total reflection frequency [Fig. 10(a)]. An attempt to take into account the weak dissipation in this system results in only one very sharp peak of the resonance interface absorption depicted in Fig. 10(b).

An interesting case is illustrated in Fig. 10(c) with only one local phonon transmission maximum (provided that dissipation is absent). This system contains an intermediate layer with weakly bound light impurities ($m_1 = 0.8m$ and $\gamma_1 = 0.093\gamma$) between tightly bound adjacent layers with not-too-heavy defect atoms ($m_2 = 1.5m$ and $\gamma_3 = 2.08\gamma$). Allowing

for weak dissipation, the absorption spectrum in such a system [Fig. 10(d)] is of the seemingly two-humped-resonance type. But in fact, only one phonon transmission channel passing through light impurities is resonant. The energy absorption in the second channel is pronounced in all the frequency domain and acts as a background for the more noticeable resonance in the first channel.

Finally, if within a nondissipative phonon spectrum only one total transmission frequency ω_T exists in the close proximity to the total reflection frequency ω_R [see Fig. 11(a)], then, allowing for weak energy dissipation, the phonon reflection and transmission coefficients may become equal to zero simultaneously, causing a double-humped resonance to be transformed into an anomalous total interface absorption [see Fig. 11(b)]. The numerical calculations for the case, presented in Fig. 11, were carried out using such parameters that correspond to a triple defect layer composed of two strongly coupled dense outer layers and a weakly coupled inner layer with very close intrinsic frequencies. In this case, the distance between the resonance frequencies ω_R and ω_T turns out small and may be compared in value with the characteristic phonon attenuation coefficient, which cannot be neglected. Note that the characteristic frequency $\omega_c = \omega_{ph}/4$ is almost equal to ω_R and ω_T; nevertheless the anomalous total interface absorption is scarcely affected by time dispersion.

The analytical calculations for total phonon interface absorption by a two-dimensional dissipative triple defect layer result in the following conditions to be satisfied:

$$[\gamma_2^2 + 4\gamma(\gamma - \gamma_2)\omega_R^2\omega_{ph}^{-2}][4m_2(\gamma_1 - i\gamma_1') - m_1(\gamma_3 - i\gamma_3')]$$

$$= 2m\gamma_2(\gamma_1 - i\gamma_1')\left(2\gamma - \gamma_2 + i\gamma_2\sqrt{\omega_{ph}^2\omega_R^{-2} - 1}\right), \quad (51)$$

$$\mathrm{Im}(\omega_R) = 0. \quad (52)$$

The above relations (51) and (52) mean that at the frequency $\omega = \omega_R$ the transmission and the reflection coefficients tend to zero together and, in view of Eq. (29), the interface absorption approaches unity, i.e., $\Delta A(\omega_R) = 1$. In Eqs. (51) and (52) the total interface absorption frequency ω_R is expressed in terms of the complex force constants by the formula (49) provided that renormalization of the nondissipative total reflection frequency due to dissipation is taken into account. To arrive at Eq. (51) renormalization of the nondissipative total transmission frequency ω_T is also allowed for.

From Eqs. (51) and (52) it follows that it is impossible to satisfy the conditions of anomalous phonon interface absorption by two-dimensional triple defect layer in the TL model on the subset of real parameters γ_1 and γ_3, i.e., if $\gamma_1' = \gamma_3' = 0$. At $\gamma_2 \neq \gamma$ from Eqs. (51) and (52) the expressions for complex values of $\gamma_1 - i\gamma_1'$ and $\gamma_3 - i\gamma_3'$ may be derived in an explicit form as functions of the other material parameters and total absorption frequency ω_R:

$$\gamma_1 - i\gamma_1' = \frac{m_1\omega_R^2}{8} \frac{2m_2 - mF(\gamma, \gamma_2, \omega_R)}{2m_2 + m_1 - mF(\gamma, \gamma_2, \omega_R)}, \quad (53)$$

$$\gamma_3 - i\gamma_3' = \frac{\omega_R^2}{4} \frac{[2m_2 - mF(\gamma, \gamma_2, \omega_R)]^2}{2m_2 + m_1 - mF(\gamma, \gamma_2, \omega_R)}, \quad (54)$$

where

$$F(\gamma, \gamma_2, \omega_R) = \frac{\gamma_2(2\gamma - \gamma_2) + i\gamma_2^2\sqrt{\omega_{ph}^2\omega_R^{-2} - 1}}{\gamma_2^2 + 4\gamma\omega_R^2\omega_{ph}^{-2}(\gamma - \gamma_2)}. \quad (55)$$

In the particular case $\gamma_2 = \gamma$ Eq. (55) may be rewritten as:

$$F(\gamma, \gamma_2, \omega_R) = 1 + i\sqrt{\omega_{ph}^2\omega_R^{-2} - 1},$$

and then for the values γ_1, γ_3 and γ_1', γ_3' the following exact expressions are obtained:

$$\gamma_1 = \frac{m_1\omega_R^2}{8}\left[1 - \frac{m_1}{M}(2m_2 + m_1 - m)\right], \quad (56)$$

$$\gamma_3 = \frac{\omega_R^2}{4}\left[2m_2 - m_1 - m + \frac{m_1^2}{M}(2m_2 + m_1 - m)\right], \quad (57)$$

$$\gamma_1' = 2\gamma\frac{m_1^2}{M}\frac{\omega_R}{\omega_{ph}}\sqrt{1 - \omega_R^2\omega_{ph}^{-2}}, \quad (58)$$

$$\gamma_3' = 4\gamma\left(1 - \frac{m_1^2}{M}\right)\frac{\omega_R}{\omega_{ph}}\sqrt{1 - \omega_R^2\omega_{ph}^{-2}}. \quad (59)$$

In Eqs. (56)–(59) the following designation is used:

$$M = (2m_2 + m_1)(2m_2 + m_1 - 2m) + m^2\omega_{ph}^2\omega_R^{-2}. \quad (60)$$

From Eqs. (56)–(60) the positive values of the defect force constants and dissipative coefficients may be obtained once the total absorption frequency ω_R is found experimentally. The case, presented in Figs. 11(a) and 11(b), corresponds to the situation where the relations $2m_2 \gg m\omega_{ph}\omega_R^{-1} > m > m_1$ and $\gamma_2 \simeq \gamma$ take place between the parameters appearing in Eqs. (56)–(60). The use of the above conditions in the formulas (56), (57), and (60) gives the rough estimate $4\gamma_1/\gamma_3 \sim m_1/m_2$ for defect material constants (to a first approximation). It means just that in this particular case the frequencies of the intrinsic elastic modes are almost equal and both of them are located near the total absorption frequency ω_R. It should be noted that such a situation is an exception to the general rule which follows from the foregoing and according to which the absorption resonances coincide neither with the intrinsic frequencies nor with the nondissipative total transmission and total reflection frequencies.

To sum up, a comparison of Figs. 11(a) and 11(b) shows that including the small inner frictional forces into consideration substantially modifies the phonon transmission and the phonon reflection spectra in the vicinity of resonance and gives rise to the total interface energy absorption. This phenomenon is absent from the CB model. Besides, two other peculiarities also take place only in the TL model. One of them is a possibility to interchange the position of the narrow and the broad peaks by using defect atoms with little different material constants [Figs. 8(b) and 8(d)]. Another distinctive feature is the phenomenon of triple-peaked absorption resonance which may occur in the thrice resonant vibration system with three nondissipative total transmission frequencies [Figs. 12(a)]. A situation like this may be realized when the triple defect layer consists of fairly heavy atoms and has weak coupling with adjacent host layers. In the case depicted in Fig. 12(a) the minimum total transmission frequency $\omega_{T\min} \approx \omega_1$ is associated with one of two
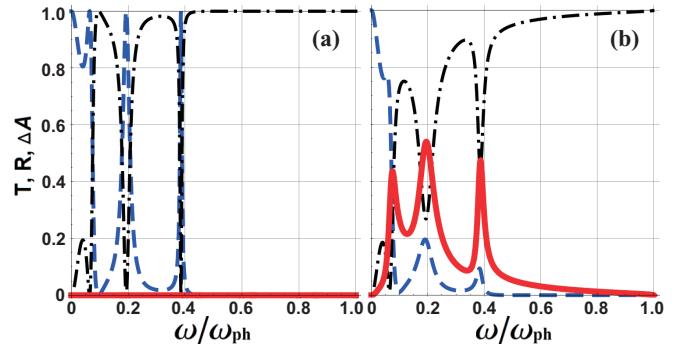

FIG. 12. Spectra of phonon energy transmission T (dashed line), reflection R (dotted-dashed line), and absorption ΔA (solid line) versus reduced frequency ω/ω_{ph} at a triple defect layer with elastic parameters $\gamma_1 = 0.05\gamma$, $\gamma_2 = 0.1\gamma$, $\gamma_3 = \gamma$ and impurity masses $m_1 = 3m$, $m_2 = 1.1m$ for the cases: (a) without dissipation and (b) with dissipative parameters $\gamma_1' = \gamma_2' = \gamma_3' = 0.00625\gamma\omega\omega_{ph}/(\omega^2 + \omega_{ph}^2/16)$.

phonon paths crossing the central defect layer. The intermediate transmission resonance $\omega_{T\mathrm{mid}} \approx \omega_2$ depends on the parameters m_2 and γ_2 characterizing the regions with one path for phonons to propagate. The maximum total transmission frequency $\omega_{T\max}$ is a function of all five parameters determining the triple defect layer. Such a nondissipative transmission spectrum [Fig. 12(a)] represents a dual interference picture in which two-path phonon interference and phonon analog of the Fabry-Pérot-type interference superpose. In a similar system, taking into account weak dissipation results in triple-peaked absorption frequency dependence [Fig. 12(b)] (see also Fig. 12 in Ref. [79] for more detail).

A. Resonance phonon interaction with homogeneous impurity monolayer between two crystals under two-channel interference conditions (FF model)

A specific case of the TL model is the FF model with an absorbed or segregated monolayer full-filled by homogeneous impurities, a second phonon path connecting straightforward two opposite edges of the host crystalline media by the next-to-nearest-neighbor force constant γ_3 (see Fig. 1 with parameters $m_2 = m$, $\gamma_2 = \gamma$, $m_1 = m_{1*}$, and $\gamma_1 = \gamma_{1*}$). In the corresponding dissipative case a double-humped interface absorption resonance is impossible, and only a single pronounced peak may exist in the phonon absorption spectrum. However this case is important for the thermal interface resistance problem. Several options of the FF model are presented in Figs. 13–15 to describe their different scattering and absorption peculiarities.

In the nondissipative crystal with a weakly bound impurity monolayer ($\gamma_1 \ll \gamma$) a two-path destructive interference manifests itself as an antiresonance dip in the close vicinity of the low intrinsic frequency ω_1 provided that the interaction γ_3 between boundary host planes is fairly strong. Figure 13(a) illustrates this case with the following parameters: $\gamma_3 = \gamma$, $\gamma_1 = 0.05\gamma$, and $m_1 = m$, a relation $\omega_T < \omega_1 \lesssim \omega_R$ being satisfied. By contrast, the weak coupling of the opposite boundary host atoms ($\gamma_3 \ll \gamma_1$) results in a total phonon transmission (resonance) through light impurity monolayer ($\omega_{ph} < \omega_R$)
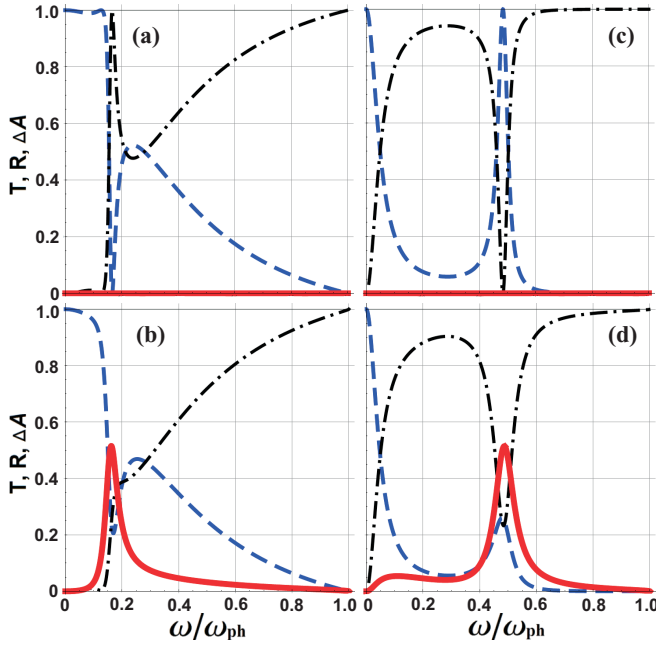
FIG. 13. Spectra of phonon energy transmission T (dashed line), reflection R (dotted-dashed line), and absorption ΔA (solid line) versus reduced frequency ω/ω_{ph} at a defect monolayer with parameters $\gamma_2 = \gamma$ and $m_2 = m$ for the cases: in (a) and (b) $\gamma_1 = 0.05\gamma$, $\gamma_3 = \gamma$ and impurity mass $m_1 = m$; in (c) and (d) $\gamma_1 = 0.09\gamma$, $\gamma_3 = 0.004\gamma$ and impurity mass $m_1 = 0.2m$; (a) and (c) without dissipation; (b) and (d) with dissipative parameters $\gamma_1' = 0.004375\gamma\omega\omega_{ph}/(\omega^2 + \omega_{ph}^2/16)$, $\gamma_3' = 0.0005\gamma\omega\omega_{ph}/(\omega^2 + \omega_{ph}^2/16)$.

observed in the neighborhood of the intrinsic frequency ω_1. Such a case is depicted in Fig. 13(c), with the parameters: $\gamma_1 = 0.09\gamma$, $\gamma_3 = 0.004\gamma$, and $m_1 = 0.2m$. For this option the inequality $\omega_1 \lesssim \omega_T$ is true. A crystal involving a similar defect layer with a narrow transmission peak in the terahertz frequency range, $\omega_T \approx 0.48\omega_{ph}$, operates as metafilter. In both extreme cases above a notable peak of interface phonon absorption may be observed in the vicinity of the intrinsic frequency at weak dissipation taken into account. Outside the
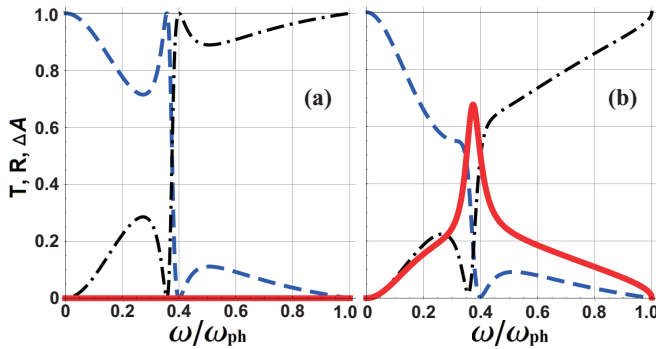

FIG. 14. Spectra of phonon energy transmission T (dashed line), reflection R (dotted-dashed line), and absorption ΔA (solid line) versus reduced frequency ω/ω_{ph} at a defect monolayer with parameters $\gamma_2 = \gamma$, $m_2 = m$, $\gamma_1 = 0.08\gamma$, $\gamma_3 = 0.8\gamma$, impurity mass $m_1 = 0.3m$ for the cases: (a) without dissipation; (b) with dissipative parameters $\gamma_1' = 0.005\gamma\omega\omega_{ph}/(\omega^2 + \omega_{ph}^2/4)$, $\gamma_3' = 0.2\gamma\omega\omega_{ph}/(\omega^2 + \omega_{ph}^2/4)$.
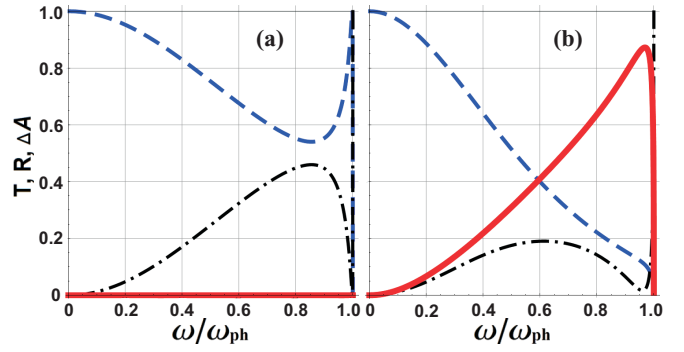

FIG. 15. Spectra of phonon energy transmission T (dashed line), reflection R (dotted-dashed line), and absorption ΔA (solid line) versus reduced frequency ω/ω_{ph} at a defect monolayer with parameters $\gamma_2 = \gamma$, $m_2 = m$, impurity mass $m_1 = 1.36m$, elastic constants $\gamma_1 = 1.16\gamma$ and $\gamma_3 = 0.88\gamma$ for the cases: (a) without dissipation, (b) with dissipative parameters $\gamma_1' = \gamma_3' = 0.2\gamma\omega\omega_{ph}/(\omega^2 + \omega_{ph}^2/4)$.

resonance frequency domain the dissipative phonon scattering characteristics differ little from ones in the lossless limit.

In the intermediate nondissipative case of weakly bound ($\gamma_1 = 0.08\gamma$) light impurities with $m_1 = 0.3m$, shown in Fig. 14(a) for fairly strong direct boundary interaction $\gamma_3 = 0.8\gamma$, one can see the closely spaced antiresonance ω_R and the constructive resonance ω_T for which the relation $\omega_T < \omega_1 < \omega_R$ is true and similar to that in the case presented in Fig. 13(a). A difference between corresponding dissipative cases can be seen in Figs. 13(b) and 14(b): Figure 14(b) illustrates the transformation of both the total reflection frequency into almost total nontransmission frequency and the total transmission frequency into almost total nonreflection frequency. Unlike such spectral behavior, in Fig. 13(b) only one almost total nonreflection resonance exists. These peculiarities are connected with different types of the time dispersion and show sensitivity to the characteristic dispersion frequency ω_c. In contrast, the absorption resonances, despite their locations, are almost independent of ω_c provided that the admissible dissipation is weak in the FF model and also in the more complicated TL model.

If the defect parameters are close to those of the host crystal, then in the high frequency domain, adjacent to the Brillouin zone edge, the lossless phonon scattering characteristics change drastically. Such a case is depicted in Fig. 15(a) with parameters: $m_1 = 1.36m$, $\gamma_1 = 1.16\gamma$, $\gamma_3 = 0.88\gamma$, the condition $\omega_R > \omega_{ph}$ being satisfied. In the respective dissipative system, Fig. 15(b), the absorption energy increases significantly with frequency at the cost of a strongly marked high-frequency drop in reflected and transmitted phonon energy. It signifies that purely dynamical approach holds only for extremely small attenuation, for example, at low temperatures. A similar 1D case without taking into account weak dissipation was discussed in Ref. [81] as applied to the problem of the thermal interface conductance at high temperatures. It is easy to make sure that the scattering characteristics in the 3D FF model are obtained from the 1D case provided the next-to-nearest-neighbor force constant γ_3 is multiplied by a factor of four. In the reasonable cases γ_3 may not exceed the host force constant γ as shown in Fig. 13(a). So, only values
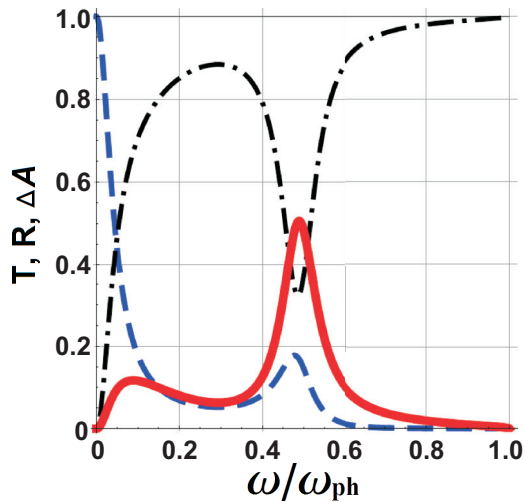
FIG. 16. Spectra of phonon energy transmission T (dashed line), reflection R (dotted-dashed line), and absorption ΔA (solid line) versus reduced frequency ω/ω_{ph} at a defect monolayer with parameters $\gamma_2 = \gamma$, $\gamma_3 = 0$, $m_2 = m$, impurity mass $m_1 = 0.2m$, elastic constant $\gamma_1 = 0.09\gamma$, and dissipative parameter $\gamma_1' = 0.00556\gamma\omega\omega_{ph}/(\omega^2 + \omega_{ph}^2/36)$.

$\gamma_3 \leqslant 0.25\gamma$ in the 1D case are to be considered as analog for the 3D model. In Ref. [81] this is not the case and γ_3 may far exceed γ. Moreover, from the above it follows that the results in 1D models should be carefully verified so as to find out if they are reliable when weak dissipation is allowed for.

If $\gamma_3 = 0$, then no direct bonds between perfect semi-infinite elastic media are allowed for and only a single path exists for phonons to penetrate the defect layer, namely, via impurities. In a particular lossless case with defect parameters as in Fig. 13(c) but at $\gamma_3 = 0$ the scattering curves appear to show the same behavior, i.e., a destructive interference antiresonance is absent and the total transmission frequency ω_T is close to almost the same intrinsic frequency $\omega_1 \lessgtr \omega_T$. In the dissipative system, corresponding to Fig. 13(d) at $\gamma_3 = \gamma_3' = 0$, the phonon absorption spectrum is almost the same as in this figure. In another dissipative single-channel system, corresponding to Fig. 13(c) at $\gamma_3 = \gamma_3' = 0$ and presented in Fig. 16, the interface absorption curve in the vicinity of the resonance frequency is nearly the same as in the first option and in the initial model with two-path phonon interference. However, it differs from the two cases above by time dispersion. In specific cases, time dispersion may result in a peculiarity, illustrated in Fig. 16, where the interface absorption curve has a small bulge in the low frequency domain apart from much more pronounced resonance in the vicinity of ω_1. Therefore, one could make a fallacy that double-humped resonance may be found also in this case. However the small low-frequency peak arises from dissipative motion of the two opposite boundaries of the host semi-infinite crystals. The contribution of this kind forms a small background in all the options of the CB model discussed in this paper. But it may not always be separated analytically out of integrated collective motion or perceptible in numerical calculations, as it was in the case analyzed in Sec. III B, where a small background is noticeable in Fig. 5(b) and given by Eq. (32). In the case of the

FF model the dissipative motion of the host crystal boundaries is responsible for absorption in one of the two parallel phonon channels by definition.

V. DISCUSSION AND CONCLUSIONS

The main conclusion of the present investigation is that no straightforward analogies exist between doubly resonant dissipative vibration systems and doubly resonant electromagnetic structure exhibiting both induced transparency and superscattering [32]. This conclusion is due to different paradigms for description of these phenomena. To obtain in the phonon dynamics the most convenient counterpart of double-humped spectral behavior of a cross section in a doubly resonant two-slits system [32], a model is presented in which an internal crystal plane is filled with impurities of two sorts alternating in staggered order. In such a system, the double-humped (double-peaked) resonance, at which the narrow peak is placed against the background of the broad hump, may occur in the interface phonon absorption due to two-path phonon interference at weak dissipation taken into account. The phononic and electromagnetic systems under comparison are described by the same number of parameters, namely six (four material and two dissipative), and have similar features in the corresponding spectral frequency dependencies: height/location of the narrow and broad peaks and Lorentzian approximation of the curves in the vicinity of their maxima. In this way we use an approximate representation of the interface phonon absorption as a sum of three terms: the losses in both channels passing through different defect bonds and the losses resulting from viscous motion of the boundary planes. But the resonance frequencies of total and zero absorptions as analogs of electromagnetic induced transparency and superscattering are not found in this proposed phononic model.

Another dissipative model, in which two-path phonon interference reveals itself as double-humped (double-peaked) resonance in the interface phonon absorption, includes a triple defect layer containing a homogeneous inner monolayer in-between two identical outer layers. This model differs from the checkerboard-type model in the following remarkable features. In the triple-defect-layer model the total interface absorption occurs provided that the energies of the transmitted and reflected phonons tend to zero at the common frequency, for example, when the intrinsic frequency of two strongly coupled dense outer layers is close to that of a weakly bound intermediate layer. In the general case the total absorption conditions give real and imaginary parts of the force constants with allowance made for resonance frequency renormalization due to weak dissipation. Also, in two cases differing a little in the defect material parameters, the absorption may peak narrowly on the opposite sides of the broad hump, whereas in the checkerboard-type model discussed in Sec. III, the narrow peak, as a rule, is to the left of the broad peak. The foregoing peculiarities of the triple-defect-layer model arise from its description by two dissipative and five material parameters. On the whole, the suggested triple-defect-layer model is thrice resonant vibration system in which the phenomenon of triple-peaked absorption resonance may be realized provided that the relevant nondissipative limit admits the three total transmission frequencies. These properties are exhibited, for ex-

ample, when a defect layer is composed of fairly heavy atoms weakly bound to adjacent host layers. In such a system, resonance spectral behavior of the scattering and absorption characteristics is due to superposition of two-path phonon interference and phonon analog of the Fabry-Pérot-type interference.

A necessary condition for two interface absorption maxima to be caused by the two-path phonon interference is a presence of two, or more, resonance transmission frequencies (it may be total or sharp pronounce resonance) and no less than one antiresonance dip within the lossless phonon spectrum. But the above condition is not sufficient. As a rule, a narrow absorption peak is located in the frequency range where the constructive and destructive resonances are closely spaced in the nondissipative limit, whereas the broad peak is located near second constructive resonance provided that the scattering coefficient curves change steeply within this interval. By contrast, if the frequency dependencies of the nondissipative scattering coefficients are fairly monotonous, then the interface phonon absorption is insignificant in the corresponding frequency domains. In particular, this is true for the simplest checkerboard-type "isotopic defect" model discussed in Sec. III. On the other hand, once one nondissipative scattering coefficient is vanishingly small, then it remains almost so in the system with low losses and the other scattering coefficient is reduced by the value of the interface phonon absorption. Thus, the scattering resonances due to two-path phonon interference may exist at extremely weak dissipation. In this case the total lossless transmission turns into an almost total dissipative nonreflection and, similarly, the total reflection becomes an almost total nontransmission. This energy balance is disturbed by further (even insignificant) rise of vibration attenuation, resulting in a noticeable increase of the minor dissipative scattering flux. In some cases, this effect leads to restriction of resonance interface absorption.

Clearly, the phenomenon of double-humped interface energy absorption by a few-layer planar defect may be used to create fine nanoscale meta-absorbers. To make progress in the solution of this problem it is necessary to keep in mind that in a particular option of the checkerboard-type model or the triple-defect-layer model the narrow and broad absorption peaks may be separated, shifted towards low frequencies or towards the Brillouin zone edge. The broad peak may become narrow or almost fully disappear. A single sharp interface absorption resonance may be found in any place of the phonon spectrum for infinitely large number of systems with few-layer planar defects which are responsible for two-path phonon interference.

Furthermore, if the task is to control the heat flux through a few-layer planar defect at high temperatures, it is important to allow for both interface absorption peculiarities and special scattering features in the nondissipative limit (without losses), when two-path phonon interference manifests itself as total phonon transmission and total phonon reflection. It might be worth it to point out that to design high-temperature phonon metafilter or metamirror for nanoscale heat control both lossless checkerboard-type and simple triple-defect-layer models are suitable. To obtain a narrow pass band in the terahertz frequency range a more appropriate system is of the type in which two perfect crystal lattices weakly bound to a homogeneous monolayer of light impurities embedded in between are also coupled directly by weak next-to-nearest-neighbor bond. Similar spectrum may be observed in the checkerboard-type model, in which either type of defect interatomic bonds is weak, and both impurity masses are of the same order as the host atoms. Otherwise such a checkerboard-type model, where only one type of defect bonds is weak and the other is tight, shows a very narrow terahertz-frequency zero-transmission dip against the background of a very wide frequency pass band.

The type of the frequency dispersion of the small dissipative parameters exerts no effect on all studied absorption resonances arising from interaction of an incident phonon with a few-layer planar defect in a crystal. In the general case of the checkerboard-type model as well as the triple-defect-layer model the incident phonon in the interior of the planar defect transforms into such an interface two-path interference hybrid for which the resonance absorption frequencies coincide neither with the intrinsic frequencies nor with the nondissipative total transmission frequencies nor with the nondissipative total reflection frequency. For this reason, it is incorrect to look for any simple analogy of the obtained results with the famous Fano resonance [82], especially since it is a single resonance.

In conclusion, it should be noted that the case of transverse phonons in which one-component atom displacements are directed in parallel with the planar defect in Fig. 1 is identical to the case of longitudinal phonons studied in the present work. Namely, the spectral characteristics (transmission, reflection, and absorption) are topologically equivalent in the corresponding scales that take into account the difference between force constants. In particular, this is obvious from the results retrieved from MD simulations and presented in Fig. 5(a) in Ref. [38] for the simplest case of the CB model.

[1] B. A. Munk, *Frequency Selective Surfaces: Theory and Design* (Wiley, New York, 2000).

[2] G. V. Eleftheriades and K. G. Balmain, *Negative-Refraction Metamaterials: Fundamental Principles and Applications* (Wiley, Hoboken, 2005).

[3] C. Caloz and T. Itoh, *Electromagnetic Metamaterials: Transmission Line Theory and Microwave Applications* (Wiley, Hoboken, 2006).

[4] R. Marques, F. Martin, and M. Sorola, *Metamaterials with Negative Parameters* (Wiley, Hoboken, 2008).

[5] W. Cai and E. Shalaev, *Optical Metamaterials: Fundamentals and Applications* (Springer, New York, 2009).

[6] F. Capolino, *Handbook on Metamaterials* (CRC Press, Boca Raton, 2009).

[7] L. Solymar and E. Shamonina, *Waves in Metamaterials* (Oxford University Press, Oxford, 2009).

[8] U. Kreibig and M. Vollmer, *Optical Properties of Metal Clusters* (Springer, Berlin, 1995).

[9] C. F. Bohren and D. R. Huffman, *Absorption and Scattering of Light by Small Particles* (Wiley, New York, 1998).

[10] U. Kreibig and P. Zacharias, Surface plasma resonances in small spherical silver and gold particles, Z. Phys. **231**, 128 (1970).

[11] M. C. Daniel and D. Astruc, Gold nanoparticles: assembly, supramolecular chemistry, quantum-size-related properties, and applications toward biology, catalysis, and nanotechnology, Chem. Rev. **104**, 293 (2004).

[12] N. Liu, H. Liu, S. Zhu, and H. Giessen, Stereometamaterials, Nat. Photonics **3**, 157 (2009).

[13] N. Liu and H. Giessen, Coupling effects in optical metamaterials, Angew. Chem. Int. Ed. **49**, 9838 (2010).

[14] N. Liu, M. Hentschel, T. Weiss, A. P. Alivisatos, and H. Giessen, Three-dimensional plasmon rulers, Science **332**, 1407 (2011).

[15] V. A. Fedotov, M. Rose, S. L. Prosvirnin, N. Parasimakis, and N. I. Zheludev, Sharp Trapped-Mode Resonances in Planar Metamaterials with a Broken Structural Symmetry, Phys. Rev. Lett. **99**, 147401 (2007).

[16] J. A. Fan, C. H. Wu, K. Bao, J. M. Bao, R. Bardhan, N. J. Halas, V. N. Manoharan, P. Nordlander, G. Shvets, and F. Capasso, Self-assembled plasmonic nanoparticle clusters, Science **328**, 1135 (2010).

[17] M. Hentschel, M. Saliba, R. Vogelgesang, H. Giessen, A. P. Alivisatos, and N. Liu, Transition from isolated to collective modes in plasmonic oligomers, Nano Lett. **10**, 2721 (2010).

[18] J. B. Lassiter, H. Sobhani, J. A. Fan, J. Kundun, F. Capasso, P. Nordlander, and N. J. Halas, Fano resonances in plasmonic nanoclusters: Geometrical and chemical tunability, Nano Lett. **10**, 3184 (2010).

[19] M. I. Stockman, Dark-hot resonances, Nature (London) **467**, 541 (2010).

[20] S. Walia, C. M. Shah, P. Gutruf, H. Nili, D. R. Chowdhury, W. Withayachumnankul, M. Bhaskaran, and S. Sriram, Flexible metasurfaces and metamaterials: A review of materials and fabrication processes at micro- and nano-scales, Appl. Phys. Rev. **2**, 011303 (2015).

[21] N. I. Landy, S. Sajuyigbe, J. J. Mock, D. R. Smith, and W. J. Padilla, Perfect Metamaterial Absorber, Phys. Rev. Lett. **100**, 207402 (2008).

[22] N. Liu, M. Mesch, T. Weiss, M. Hentschel, and H. Giessen, Infrared perfect absorber and its application as plasmonic sensor, Nano Lett. **10**, 2342 (2010).

[23] M. Diem, T. Koschny, and C. M. Soukoulis, Wide-angle perfect absorber/thermal emitter in the terahertz regime, Phys. Rev. B **79**, 033101 (2009).

[24] H. Li, L. H. Yuan, B. Zhou, X. P. Shen, Q. Cheng, and T. J. Cui, Ultrathin multiband gigahertz metamaterial absorbers, J. Appl. Phys. **110**, 014909 (2011).

[25] V. S. Asadchy, Y. Radi, J. Vehmas, and S. A. Tretyakov, Functional Metamirrors Using Bianisotropic Elements, Phys. Rev. Lett. **114**, 095503 (2015).

[26] V. S. Asadchy, I. A. Faniayeu, Y. Radi, S. A. Khakhomov, I. V. Semchenko, and S. A. Tretyakov, Broadband Reflectionless Metasheets: Frequency-Selective Transmission and Perfect Absorption, Phys. Rev. X **5**, 031005 (2015).

[27] H.-T. Chen, A. J. Taylor, and N. Yu, A review of metasurfaces: physics and applications, Rep. Prog. Phys. **79**, 076401 (2016).

[28] A. A. Basharin, M. Kafesaki, E. N. Economou, C. M. Soukoulis, V. A. Fedotov, V. Savinov, and N. I. Zheludev, Dielectric Metamaterials with Toroidal Dipolar Response, Phys. Rev. X **5**, 011036 (2015).

[29] I. S. Spevak, A. Yu. Nikitin, E. V. Bezuglyi, Alex Levchenko, and A. V. Kats, Resonantly suppressed transmission and anomalously enhanced light absorption in periodically modulated ultrathin metal films, Phys. Rev. B **79**, 161406(R) (2009).

[30] G. Alagappan and C. E. Png, Doubly resonant optical periodic structure, Sci. Rep. **6**, 20590 (2016).

[31] M. Born and E. Wolf, *Principles of Optics* (Cambridge University Press, Cambridge, 1999), 7th ed.

[32] L. Verslegers, Z. Yu, Z. Ruan, P. B. Cattysse, and S. Fan, From Electromagnetically Induced Transparency to Superscattering with a Single Structure: A Coupled-Mode Theory for Doubly Resonant Structures, Phys. Rev. Lett. **108**, 083902 (2012).

[33] Z. Liu, X. Zhang, Y. Mao, Y. Y. Zhu, Z. Yang, C. T. Chan, and P. Sheng, Locally resonant sonic materials, Science **289**, 1734 (2000).

[34] A. Fellay, F. Gagel, K. Maschke, A. Virlouvet, and A. Khater, Scattering of vibrational waves in perturbed quasi-one-dimensional multichannel waveguides, Phys. Rev. B **55**, 1707 (1997).

[35] Yu. A. Kosevich, Capillary phenomena and macroscopic dynamics of complex two-dimensional defects in crystals, Prog. Surf. Sci. **55**, 1 (1997).

[36] A. M. Kosevich and A. V. Tutov, Peculiarities of elastic wave scattering from a planar crystal defect and pseudosurface vibrations, Phys. Lett. A **248**, 271 (1998).

[37] A. M. Kosevich, Two-channel resonance scattering of waves and particles by point and planar defects, J. Exper. and Theor. Physics **88**, 168 (1999).

[38] H. Han, L. G. Potyomina, A. N. Darinskii, S. Volz, and Yu. A. Kosevich, Phonon interference and thermal conductance reduction in atomic-scale metamaterials, Phys. Rev. B **89**, 180301(R) (2014).

[39] Yu. A. Kosevich, H. Han, L. G. Potyomina, A. N. Darinskii, and S. Volz, Phonon interference and energy transport in nonlinear lattices with resonance defects, in *Quodons in Mica*, edited by J. F. R. Archilla, Springer Series in Materials Science 221 (Springer, Heidelberg, 2015), pp. 247–263.

[40] Yu. A. Kosevich, L. G. Potyomina, A. N. Darinskii, and I. A. Strelnikov, Phonon interference control of atomic-scale metamirrors, meta-absorbers, and heat transfer through crystal interfaces, Phys. Rev. B **97**, 094117 (2018).

[41] D. A. Young and H. J. Maris, Lattice-dynamical calculation of the Kapitza resistance between fcc lattices, Phys. Rev. B **40**, 3685 (1989).

[42] S. Pettersson and G. D. Mahan, Theory of the thermal boundary resistance between dissimilar lattices, Phys. Rev. B **42**, 7386 (1990).

[43] R. J. Stoner and H. J. Maris, Kapitza conductance and heat flow between solids at temperatures from 50 to 300 K, Phys. Rev. B **48**, 16373 (1993).

[44] H. Zhao and J. B. Freund, Lattice-dynamical calculation of phonon scattering at ideal Si-Ge interfaces, J. Appl. Phys. **97**, 024903 (2005).

[45] P. Hyldgaard and G. D. Mahan, Phonon superlattice transport, Phys. Rev. B **56**, 10754 (1997).

[46] M. V. Simkin and G. D. Mahan, Minimum Thermal Conductivity of Superlattices, Phys. Rev. Lett. **84**, 927 (2000).

[47] B. Yang and G. Chen, Partially coherent phonon heat conduction in superlattices, Phys. Rev. B **67**, 195311 (2003).

[48] S.-F. Ren, W. Cheng, and G. Chen, Lattice dynamics investigations of phonon thermal conductivity of Si/Ge superlattices with rough interfaces, J. Appl. Phys. **100**, 103505 (2006).

[49] D. L. Nika, E. P. Pokatilov, A. A. Balandin, V. M. Fomin, A. Rastelli, and O. G. Schmidt, Reduction of lattice thermal conductivity in one-dimensional quantum-dot superlattices due to phonon filtering, Phys. Rev. B **84**, 165415 (2011).

[50] E. T. Swartz and R. O. Pohl, Thermal boundary resistance, Rev. Mod. Phys. **61**, 605 (1989).

[51] S. M. Lee, D. G. Cahill, and R. Venkatasubramanian, Thermal conductivity of Si-Ge superlattices, Appl. Phys. Lett. **70**, 2957 (1997).

[52] W. S. Capinski, H. J. Maris, T. Ruf, M. Cardona, K. Ploog, and D. S. Katzer, Thermal-conductivity measurements of GaAs/AlAs superlattices using a picosecond optical pump-and-probe technique, Phys. Rev. B **59**, 8105 (1999).

[53] B. Yang and G. Chen, Lattice dynamics study of anisotropic heat conduction in superlattices, Microscale Thermophys. Eng. **5**, 107 (2001).

[54] P. L. Kapitza, The study of heat transfer in helium II, Zh. Eksp. Teor. Fiz. **11**, 1 (1941) [J. Phys. (USSR) **4**, 181 (1941)].

[55] Z. Zhang, *Nano/Microscale Heat Transfer* (McGraw-Hill, New York, 2007).

[56] S. Volz, R. Carminati, P. Chantrenne, S. Dilhaire, S. Gomez, N. Trannoy, and G. Tessier, *Microscale and Nanoscale Heat Transfer* (Springer, Berlin, 2007).

[57] S. Volz, *Thermal Nanosystems and Nanomaterials*, Topics in Applied Physics 118 (Springer-Verlag, Berlin/Heidelberg, 2009).

[58] E. S. Toberer, L. L. Baranowski, and C. Dames, Advances in thermal conductivity, Annu. Rev. Mater. Res. **42**, 179 (2012).

[59] D. G. Cahill, W. K. Ford, K. E. Goodson, G. D. Mahan, A. Majumdar, H. J. Maris, R. Merlin, and S. R. Phillpot, Nanoscale thermal transport, J. Appl. Phys. **93**, 793 (2003).

[60] D. G. Cahill, P. V. Braun, G. Chen, D. R. Clarke, S. Fan, K. E. Goodson, P. Keblinski, W. P. King, G. D. Mahan, A. Majumdar, H. J. Maris, S. R. Phillpot, E. Pop, and L. Shi, Nanoscale thermal transport. II. 2003-2012, Appl. Phys. Rev. **1**, 011305 (2014).

[61] N. Li, J. Ren, L. Wang, G. Zhang, P. Hanggi, and B. Li, Colloquium: Phononics: Manipulating heat flow with electronic analogs and beyond, Rev. Mod. Phys. **84**, 1045 (2012).

[62] A. Feher, A. A. Mamalui, A. Ya. Dul'fan, E. S. Syrkin, and A. G. Shkorbatov, Low-temperature phonon transport in 3D point-contacts (Review), Low Temp. Phys. **31**, 921 (2005).

[63] B. C. Daly, H. J. Maris, K. Imamura, and S. Tamura, Molecular dynamics calculation of the thermal conductivity of superlattices, Phys. Rev. B **66**, 024301 (2002).

[64] E. S. Landry and A. J. H. McGaughey, Thermal boundary resistance predictions from molecular dynamics simulations and theoretical calculations, Phys. Rev. B **80**, 165304 (2009).

[65] Y. Chen, D. Li, J. Yang, Y. Wu, J. R. Lukes, and A. Majumdar, Molecular dynamics study of the lattice thermal conductivity of Kr/Ar superlattice nanowires, Physica B **349**, 270 (2004).

[66] M. Hu, P. Keblinski, and P. K. Schelling, Kapitza conductance of silicon-amorphous polyethylene interfaces by molecular dynamics simulations, Phys. Rev. B **79**, 104305 (2009).

[67] R. J. Stevens, L. V. Zhigilei, and P. M. Norris, Effects of temperature and disorder on thermal boundary conductance at solid-solid interfaces: Nonequilibrium molecular dynamics simulations, Int. J. Heat Mass Transfer **50**, 3977 (2007).

[68] K. Sääskilahti, J. Oksanen, J. Tukki, and S. Volz, Role of anharmonic phonon scattering in the spectrally decomposed thermal conductance at planar interfaces, Phys. Rev. B **90**, 134312 (2014).

[69] N. Mingo and L. Yang, Phonon transport in nanowires coated with an amorphous material: An atomic Green's function approach, Phys. Rev. B **68**, 245406 (2003).

[70] J.-S. Wang, J. Wang, and N. Zeng, Nonequilibrium Green's function approach to mesoscopic thermal transport, Phys. Rev. B **74**, 033408 (2006).

[71] J.-S. Wang, N. Zeng, J. Wang, and Ch. K. Gan, Nonequilibrium Green's function method for thermal transport in junctions, Phys. Rev. E **75**, 061128 (2007).

[72] N. Mingo, Green's function methods for phonon transport through nano-contacts, in *Thermal Nanosystems and Nanomaterials*, edited by S. Volz, Topics in Applied Physics 118 (Springer-Verlag, Berlin/Heidelberg, 2009), pp. 63–94.

[73] P. E. Hopkins and P. M. Norris, Effects of joint vibrational states on thermal boundary conductance, Nanoscale Microscale Thermophys. Eng. **11**, 247 (2007).

[74] P. E. Hopkins, J. C. Duda, and P. M. Norris, Anharmonic phonon interaction at interfaces and contributions to thermal boundary conductance, ASME J. Heat Transfer **133**, 062401 (2011).

[75] P. E. Hopkins, Multiple phonon processes contributing to inelastic scattering during thermal boundary conductance at solid interfaces, J. Appl. Phys. **106**, 013528 (2009).

[76] P. E. Hopkins and P. M. Norris, Relative contributions of inelastic and elastic diffuse phonon scattering to thermal boundary conductance across solid interfaces, ASME J. Heat Transfer **131**, 022402 (2009).

[77] P. M. Norris and P. E. Hopkins, Examining interfacial diffuse phonon scattering through transient thermoreflectance measurements of thermal boundary conductance, J. Heat Transfer **131**, 043207 (2009).

[78] L. D. Landau and E. M. Lifshitz, *Mechanics* (Butterworth-Heinemann, Oxford, 2000).

[79] See Supplemental Material at http://link.aps.org/supplemental/10.1103/PhysRevB.102.174315 for another version of the figures in a larger scale and with additional panels for the maximum sharpness.

[80] K. N. Zinov'eva, Peculiar features of acoustic energy transmission from liquid helium to metals, Low Temp. Phys. **23**, 355 (1997).

[81] H. Han, L. Feng, S. Xiong, T. Shiga, J. Shiomi, S. Volz, and Yu. A. Kosevich, Effects of phonon interference through long range interatomic bonds on thermal interface conductance, Low Temp. Phys. **42**, 711 (2016).

[82] U. Fano, Effects of configuration interaction on intensities and phase shifts, Phys. Rev. **124**, 1866 (1961).